

NUCLEAR SPIN RESONANCE

V. S. GRECHISHKIN and N. E. AĬNBINDER

Usp. Fiz. Nauk 80, 597-637 (August, 1963)

I. Introduction	566
II. NSR energy levels and frequencies.	568
1. Energy levels for resonating nuclei with spins 1 or $\frac{3}{2}$	568
2. NSR energy levels for spin $\frac{5}{2}$	571
III. Relative intensities of NSR lines	571
1. Relative intensities of Zeeman components in NQR.	571
2. Generalized NSR equations.	572
3. Relative intensities of NSR lines for spin 1 or $\frac{3}{2}$	572
4. Relative intensities of NSR lines for spin $\frac{5}{2}$	577
IV. Temperature dependence of the absorption frequencies and theory of nuclear spin-lattice relaxation.	578
V. Experimental procedure.	581
VI. Experimental values of the quadrupole interaction constants	582
Cited literature	587

I. INTRODUCTION

THE first experimental studies of nuclear quadrupole interactions in crystals were carried out in 1950, when Pound^[1] investigated in detail some features of the splitting of nuclear magnetic resonance lines due to the quadrupole interaction constants and Dehmelt and Kruger^[2] observed absorption of radio waves in zero magnetic field. These two pioneering investigations determined the research that followed. One of the resultant trends involved large quadrupole interaction constants and weak magnetic fields (so-called nuclear quadrupole resonance) while the other involved strong magnetic fields and quadrupole couplings (nuclear magnetic resonance split by quadrupole interaction). For almost eight years the development of both theory and experiment followed these trends, and important results were obtained to turn these methods into a new means of structural analysis of single crystals. Dozens and hundreds of papers were published both on nuclear quadrupole resonance (particularly in zero magnetic field) and on nuclear magnetic resonance split by quadrupole interaction. In the case of nuclear quadrupole resonance (NQR), the energy of the magnetic interaction with the external magnetic field H_0 can be regarded as a perturbation to the quadrupole energy, so that it is possible to calculate relatively easily by perturbation theory the energy levels and their dependence on the angles between the direction of H_0 and the principle axes of the electric field gradient tensor of the crystal. The theory for nuclear magnetic resonance (NMR) is constructed analogously, but in this case the perturbation is the quadrupole interaction energy. A detailed discussion of all the questions connected with these trends can be found in the literature. Thus, NQR is dealt with by

Grechishkin^[3], Das and Hahn^[4], and Fedin and Semin^[5]. The study of quadrupole effects in NMR is treated in the review by Cohen and Reif^[6], and briefly in the books by Andrew^[7] and Lösche^[8].

In 1958^[9,10] calculations and experiments were performed for the case when the quadrupole and magnetic interactions were of the same order. It is possible to introduce a dimensionless parameter $R = 4\mu H_0 / eQq_{zz}$, where eQq_{zz} is the quadrupole coupling constant and μ is the magnetic moment of the nucleus. Obviously, $R \ll 1$ and $R \gg 1$ correspond to NQR and NMR respectively. The case $R \sim 1$ is called nuclear spin resonance (NSR).

Since the experiments made in weak and strong fields* have been sufficiently well described in our literature, we touch upon them only briefly, paying principal attention to intermediate fields. We note that there is no such review in the foreign literature, although the theoretical and experimental material accumulated by now is already quite extensive.

In order to make the exposition that follows more understandable, we shall dwell briefly on quadrupole effects in NMR and the Zeeman effect in NQR. Nuclei with spin larger than $\frac{1}{2}$ can have, in addition to a magnetic dipole moment, also an electric quadrupole moment, which is a measure of the deviation of the shape of the nucleus from spherical. Such nuclei, interacting with the intracrystalline electric fields, can produce complicated spectral patterns when a permanent magnetic field is applied. This question was first investigated by Pound^[1] who showed that when the gradient of the electric field had axial symmetry the resonance spectrum in the single crystal was split by

*Magnetic fields are called weak or strong if $4\mu H_0 \ll eQq_{zz}$ or $4\mu H_0 \gg eQq_{zz}$, respectively.

the quadrupole effects into 2J components ($J = \text{spin}$). For example, in resonance of Na^{23} ($J = 3/2$) in a single crystal of NaNO_3 , a triplet was observed in a strong magnetic field, the splitting reaching in NaNO_3 several times ten kcs, which is much larger than the dipole-dipole line width.

Using first-order perturbation theory, it is easy to obtain the following expression for the frequencies of the spectrum:

$$\nu_{m \rightarrow m-1} = \nu_0 + \frac{3eQq_{zz}(2m-1)}{8J(2J-1)}(3 \cos^2 \theta - 1), \quad (1)$$

where m — magnetic quantum number, $\nu_0 = \mu H_0 / J$ — NMR frequency in the absence of quadrupole effects, eQq_{zz} — quadrupole coupling constant, μ — magnetic moment of the nucleus, J — spin of the nucleus, and θ — angle between the symmetry axis of the electric field and the direction of the external magnetic field H_0 . Pound measured the splitting between the central and side components as a function of θ and found that $\Delta\nu = 83.5(3 \cos^2 \theta - 1)$ kcs for NaNO_3 . Hence $1/4 eQq_{zz} = 83.5$ kcs.

Analogous investigations were made also in Al_2O_3 for Al^{27} nuclei ($J = 5/2$), with five spectrum components observed. As θ was varied, the central component of the spectrum also shifted, owing to second-order effects (the splitting amounted to 25 percent of the central frequency, and first-order perturbation theory was no longer valid). However, Pound considered only the relatively rarely encountered case of an axially symmetrical electric field gradient. Therefore Volkoff constructed a theory for the more general case of arbitrary electric field symmetry^[11]. Volkoff's method makes it possible to determine the direction of the principal axes of the electric field gradient relative to the principle axes of the crystal, and to measure eQq_{zz} and $\eta = (q_{xx} - q_{yy})/q_{zz}$ (the asymmetry parameter), where q_{xx} , q_{yy} , and q_{zz} are the components of the electric field gradient tensor of the crystal.

In this method, three arbitrary mutually perpendicular axes X, Y, and Z are chosen in the crystal. Let X, Y, and Z have direction cosines λ_i , μ_i , and ν_i with respect to the principal axes of the electric field gradient tensor. By examining the symmetry of the crystal lattice it is frequently possible to align one of the principal axes of the electric field gradient tensor with the crystal axis. If H_0 is alternately directed perpendicular to X, Y, or Z and if the crystal is rotated each time around the H_0 direction, then first-order perturbation theory gives the following expression for the splitting $2\Delta\nu$ between two spectral components due to the transitions $m \rightarrow m-1$ and $-(m-1) \rightarrow -m$:

$$2\Delta\nu = A + B \cos 2\theta + C \sin \theta, \quad (2)$$

where for rotation of the crystal about the x axis we have

$$\left. \begin{aligned} A_x &= 2k \left[\frac{1}{2} - \frac{3}{2} \lambda_3^2 + \frac{1}{2} \eta (\lambda_2^2 - \lambda_1^2) \right], \\ B_x &= 2k \left[\frac{3}{2} (\mu_3^2 - \nu_3^2) + \frac{1}{2} \eta (\mu_1^2 - \nu_1^2 - \mu_2^2 + \nu_2^2) \right], \\ C_x &= 2k [-3\mu_3\nu_3 + \eta (\mu_2\nu_2 - \mu_1\nu_1)], \\ k &= eQq_{zz} \left[\frac{3(2m-1)}{8J(2J-1)} \right], \end{aligned} \right\} \quad (3)$$

m is the largest magnetic quantum number.

It can be shown that

$$\left. \begin{aligned} A_x + A_y + A_z &= 0, & A_z - B_z &= A_x + B_x, \\ A_y - B_y &= A_z + B_z, & A_x - B_x &= A_y + B_y. \end{aligned} \right\} \quad (4)$$

Carrying out all three rotations, we can easily obtain the coefficients A, B, and C. Therefore, by solving the system of algebraic equations (3), we obtain all the structural parameters.

The possibilities of this method were demonstrated with spodumene $\text{LiAl}(\text{SiO}_3)_2$ as an example^[11].

For the resonance of the Li^7 nucleus ($J = 3/2$) in this crystal, they obtained

$$\begin{aligned} \eta &= 0.793, & |k| &= 18.9 \text{ kcs}, & eQq_{zz} &= 75.6 \text{ kcs} \\ \lambda_1 &= -0.074, & \lambda_2 &= 0.997, & \lambda_3 &= 0.020, \\ \mu_1 &= 0.746, & \mu_2 &= 0.042, & \mu_3 &= 0.665, \\ \nu_1 &= 0.662; & \nu_2 &= 0.065; & \nu_3 &= -0.747, \end{aligned}$$

with the X axis coinciding with the b axis of monoclinic spodumene ($C_y = C_z = 0$), and the Z axis, chosen as the direction perpendicular to b and c, so that the a axis was between Y and Z.

Calculations of higher-order perturbations were carried out by Volkoff^[11] and also by Bersonn^[13]. These calculations were also experimentally confirmed for the resonance of Al^{27} ($J = 5/2$) in spodumene^[14,15].

Volkoff's method is presently widely used, for it gives the frequencies as functions of the angles of rotation in a Cartesian frame.

Euler angles are used in the method of Itoh and his co-workers^[16]. This method is more complicated than Volkoff's and offers no advantages over the latter with respect to the accuracy with which the constants are determined. In practice, Itoh's method was used only for the resonance of Na^{23} ($J = 3/2$) in sodium thio-sulfate ($\text{Na}_2\text{S}_2\text{O}_3 \cdot 5\text{H}_2\text{O}$), whereas Volkoff's method was used not only for spodumene but for other objects, for example the resonance of B^{11} ($J = 3/2$) in kernite $\text{Na}_2\text{B}_4\text{O}_7 \cdot 4\text{H}_2\text{O}$,^[17] for Al^{27} in HBeAlSiO_5 ,^[18] etc.

Finally, Brown and Williams^[19,20] analyzed the spectrum of Be^9 ($J = 3/2$) in beryl $\text{Be}_3\text{AlSi}_6\text{O}_{18}$. Their method, however, yielded results only for the case when the magnetic field H_0 was parallel to the principal axes.

Kornfel'd and Lemanov^[21] studied the intensity of satellites in mixed $\text{NaNO}_3 - \text{AgNO}_3$ crystals as a function of the AgNO_3 content. They showed that the critical-sphere model is applicable (see, for exam-

ple,^[3]) and found that its radius was equal to 13 Å.* Thus, the intensities of the satellites of the main line characterize the degree of order in the crystal, a fact which can be used to study solid solutions or plastically deformed crystals.^[22]

Lemanov^[23], for example, studied the effect of elastic deformation on the Na²³ absorption line in rock salt crystals and determined the components of the tensor that relates the elastic deformation of the lattice with the electric field gradient.

We shall not consider here the numerous results obtained in strong fields, since they can be found elsewhere^[6].

We now stop briefly to discuss the data obtained in weak magnetic fields (NQR). The theory of the Zeeman effect in NQR for the case $\eta = 0$ was first developed by Bersonn^[13], who also used perturbation theory methods. Dean^[24] discussed especially the case of spin $\frac{3}{2}$. Cohen^[25] made numerical calculations for spins $\frac{5}{2}$, $\frac{7}{2}$, and $\frac{9}{2}$.

The following expression was obtained for the energy levels.

$$E_{\pm m} = E_{\pm m}(0) \pm \frac{\gamma h H_0}{2} [a_m^2 \cos^2 \theta + (b_m^2 + c_m^2 + 2b_m c_m \cos 2\varphi) \sin^2 \theta]^{1/2}, \quad (5)$$

where $E_{\pm m}(0)$ —value of the energy at $H_0 = 0$, γ —gyromagnetic ratio of the nucleus, m —magnetic quantum number, and

$$\left. \begin{aligned} a_m &= 2m, \\ b_{1/2} &= J + \frac{1}{2}, \quad b_m = 0 \quad \left(\text{for } m > \frac{1}{2} \right), \\ c_{1/2} &= -c_{3/2} = -\left(J - \frac{1}{2} \right) \left(J + \frac{1}{2} \right) \left(J + \frac{3}{2} \right) \frac{\eta}{6}, \\ c_m &= 0 \quad \left(\text{for } m > \frac{3}{2} \right). \end{aligned} \right\} \quad (6)$$

From this we can obtain for the transition frequencies

$$\omega = \omega_Q (m_1 \rightarrow m_2) \pm \frac{\gamma H_0}{2} ([m_1] \pm [m_2]), \quad (7)$$

where

$$[m] = [a_m^2 \cos^2 \theta + (b_m^2 + c_m^2 + 2b_m c_m \cos 2\varphi) \sin^2 \theta]^{1/2}. \quad (8)$$

Thus, two pairs of lines are observed for $J = \frac{3}{2}$. The pair with the larger splitting ($\gamma H_0([m_1] + [m_2])$) is called the β pair, while the pair with the smaller splitting is called the α pair. We see from (7) that the α pair becomes a singlet when $[m_1] = [m_2]$ (Fig. 1). For the $\frac{1}{2} \rightleftharpoons \frac{3}{2}$ transitions the zero-splitting region depends on the angles θ and φ , and forms a cone around the Z axis. The angle between H_0 and Z has for zero splitting a maximum in the XZ plane and a minimum in the YZ plane, where X, Y, and Z are the principal axes of the electric field gradient tensor.

*The critical sphere is defined as a volume inside the crystal, surrounding the impurity, in which the effect of the impurity ion on the resonating nuclei is such that their frequencies shift outside of the resonance line.

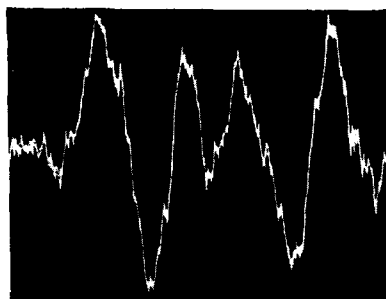


FIG. 1. NQR spectrum of Cl³⁵ in the single crystal β -n-C₆H₄Cl₂.

Therefore, using the method of the zero-splitting cone^[24], we can determine the directions of X, Y, and Z. On the other hand, knowledge of θ_0 in two planes [$\theta_0(\varphi = 0^\circ)$ and $\theta_0(\varphi = 90^\circ)$] makes it possible to calculate the asymmetry parameter

$$\eta = 3 \frac{\sin^2 \theta_0(0^\circ) - \sin^2 \theta_0(90^\circ)}{\sin^2 \theta_0(0^\circ) + \sin^2 \theta_0(90^\circ)}. \quad (9)$$

Relations (7)–(9) were used for structural analysis of some single crystals. We note that nuclear spin resonance in powders can not usually be observed, since the spectrum is smeared there over a broad region.

The Zeeman effect in NQR was investigated for Cl³⁵ in the single crystal NaClO₃ in ^[7-9] and yielded the structural data. This method was used to study some 20 crystals. A more detailed discussion of the Zeeman effect in NQR can be found in ^[4].

Thus, the theory for both strong and weak magnetic fields was developed by using perturbation theory. If eQq_{zz} is sufficiently large (for example, for organic compounds of chlorine), NMR split by quadrupole interactions cannot be realized by presently available means (attainable magnetic fields). It is then convenient to use the method of weak magnetic fields. However, for medium values of eQq_{zz} it is possible, by varying the magnetic field, to trace continuously the transition from NQR to NMR and vice versa. It will be shown below that many interesting phenomena can be observed in the intermediate region, for example the crossing of the energy levels, and these can be used for structure determinations.

In the present review we report primarily the results for intermediate magnetic fields, where perturbation theory can no longer be used and the problem is thus considerably complicated. We note that the region of intermediate fields was discussed very briefly in ^[3,4,6].

II. NSR ENERGY LEVELS AND FREQUENCIES

1. Energy Levels for Resonating Nuclei with Spin 1 or $\frac{3}{2}$.

We consider some theoretical results for intermediate magnetic fields, where perturbation theory cannot be used. If the asymmetry parameter $\eta = 0$ and the magnetic field lies in the XZ plane, then the solu-

tion of the problem entails no particular difficulty^[29]. In the case of arbitrary η and arbitrary direction of H_0 relative to the principal axes of the electric field gradient tensor, the calculation becomes much more complicated^[30]. We shall not discuss the procedure for obtaining the spin Hamiltonian, since it was described in the reviews^[4,6], and present it in the form obtained in^[30]:

$$\mathcal{H} = \frac{eQq_{zz}}{4J(2J-1)} \left[(3I_z^2 - I^2) + \frac{\eta}{2} (I_+^2 + I_-^2) \right] - g\beta H_0 \left(I_z \cos \theta + \frac{I_+ + I_-}{2} \sin \theta \cos \varphi + \frac{I_+ - I_-}{2j} \sin \theta \sin \varphi \right), \quad (10)$$

where I_z , I_+ , and I_- are the projection operators of the mechanical momentum of the nucleus I , g the nuclear gyromagnetic factor, β the nuclear magneton, θ the angle between H_0 and Z , and φ the azimuth angle.

The matrix elements of the mechanical momentum can be calculated from the formulas^[31,32]

$$\left. \begin{aligned} (m | I_z | m) &= m, \\ (J, m | I^2 | J, m) &= J(J+1), \\ (J, m | I_{\pm}^2 | J, m \mp 2) &= [(J \pm m)(J \pm m - 1)(J \mp m + 1)(J \mp m + 2)]^{1/2}, \\ (\bar{J}, m | I_{\pm} | J, m \mp 1) &= [(J \pm m)(J \pm m + 1)]^{1/2}. \end{aligned} \right\} \quad (11)$$

If $J = 1$, then the matrix of the Hamiltonian (10) is written in the form

$$eQq_{zz} \begin{pmatrix} a & b & c \\ b & d & e \\ e & c & f \end{pmatrix} \quad (12)$$

with elements

$$\left. \begin{aligned} a &= \frac{1}{4} - \frac{R}{4} \cos \theta, & d &= \frac{1}{4} + \frac{R}{4} \cos \theta, \\ b &= \frac{\eta}{4}, & e &= -\frac{R}{4\sqrt{2}} (\sin \theta \cos \varphi - j \sin \theta \sin \varphi), \\ c &= -\frac{R}{4\sqrt{2}} (\sin \theta \cos \varphi + j \sin \theta \sin \varphi), & f &= -\frac{1}{2}, \end{aligned} \right\} \quad (13)$$

where $R = 4\mu H_0 / eQq_{zz}$ and μ is the magnetic moment of the nucleus. The rows and the columns of the matrix (12) correspond to the magnetic quantum numbers $m = +1, -1$, and 0 . The parameter R can assume values from 0 to ∞ . To find the NSR energy levels it is necessary to diagonalize the matrix, i.e., to solve a third-degree determinant. With an electronic computer it is not too difficult to solve such a problem for specific research objects. In some cases, however, the problem can be solved rigorously. For resonating nuclei with spins $J = 1$ or $J = 3/2$ this can be done if the magnetic field is parallel to one of the principal axes of the electric field gradient tensor, X , Y , or Z . For $J = 1$ we can obtain^[30]:

1) If $\theta = 0$ and $\varphi = 0$, then the solution of the secular equation is written in the form

$$\left. \begin{aligned} \lambda_{1,2} &= \left(\frac{1}{4} \pm \frac{1}{4} \sqrt{\eta^2 + R^2} \right) eQq_{zz}, \\ \lambda_3 &= -\frac{1}{2} eQq_{zz}. \end{aligned} \right\} \quad (14)$$

2) Analogously, for $\theta = \pi/2$ and $\varphi = 0$

$$\left. \begin{aligned} \lambda_{1,2} &= \left(-\frac{1-\eta}{8} \pm \frac{1}{8} \sqrt{(3+\eta)^2 + 4R^2} \right) eQq_{zz}, \\ \lambda_3 &= \left(\frac{1}{4} - \frac{\eta}{4} \right) eQq_{zz}. \end{aligned} \right\} \quad (15)$$

3) For $\theta = \pi/2$ and $\varphi = \pi/2$ we obtain

$$\left. \begin{aligned} \lambda_{1,2} &= \left(-\frac{1+\eta}{8} \pm \frac{1}{8} \sqrt{(3-\eta)^2 + 4R^2} \right) eQq_{zz}, \\ \lambda_3 &= \left(\frac{1}{4} + \frac{\eta}{4} \right) eQq_{zz}. \end{aligned} \right\} \quad (16)$$

In urea $CO(NH_2)_2$ we have $eQq_{zz} = 3.5$ Mc for N^{14} ($J = 1$) and $\eta = 0.324$ ^[30,33]. The numerical results for this compound are given in Fig. 2.

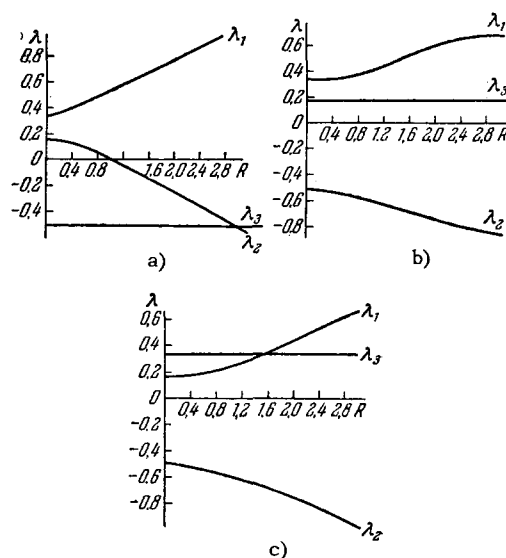


FIG. 2. NSR energy levels in single crystal of urea (N^{14} resonance).

a) $\theta = 0, \varphi = 0$; b) $\theta = \frac{\pi}{2}, \varphi = 0$; c) $\theta = \frac{\pi}{2}, \varphi = \frac{\pi}{2}$.

It will be made clear in what follows that in this case transitions between any pair of levels are possible. The frequency $\nu_{3,1}$ increases with increasing R , while $\nu_{3,2}$ decreases (Fig. 2a). This makes it possible to observe when the frequencies $\nu_{3,1}$ and $\nu_{3,2}$ coincide with the frequency $\nu_{2,1}$, $\nu_{3,1} = \nu_{2,1}$ for $R = \sqrt{1-\eta^2}$ or for $H_0 = (eQq_{zz}/4\mu) \sqrt{1-\eta^2}$. However, this case is difficult to investigate experimentally. A simpler case is the equality $\nu_{3,1} = \nu_{2,1}$ which is realized for $R = \sqrt{9-\eta^2}$ (point of level crossing) or for $H_0 = (eQq_{zz}/4\mu) \sqrt{9-\eta^2}$. In this case a single line should be observed at a frequency $\nu_{2,1} = 3/2 eQq_{zz}$ (~ 5.2 Mc). Measurement of the frequency $\nu_{2,1}$ at this point yields the asymmetry parameter η and the quadrupole coupling constant

$$\eta = \sqrt{9 - \left(\frac{6\mu H_0}{\nu_{2,1}} \right)^2}. \quad (17)$$

In urea, one of the nuclear resonance frequencies becomes equal to the proton resonance frequency at $H_0 = 450$ or 700 Oe. This equalization of the frequencies of systems of different levels should stimulate spin-spin interaction between the protons and nuclei of the

nitrogen. Such a system is analogous to resonant radio circuits tuned to the same frequency, and "pumping" of energy from one nuclear spin system to the other can be expected in this case. Since the spin-lattice relaxation time of the nitrogen nuclei is shorter than the proton relaxation time (due to the quadrupole effect) the relaxation time of the hydrogen nuclei will become shorter. These questions will be considered later on. In the case $\theta = \pi/2$ and $\varphi = \pi/2$, the levels λ_1 and λ_3 cross at the point $R = \sqrt{2\eta^2 + 6\eta}$. Thus, the position of the crossing points is determined uniquely by the value of the asymmetry parameter. In the latter case (Fig. 2c) the crossing of the levels for urea occurs in a magnetic field ~ 4170 Oe. Then a singlet should be observed at $\nu = 3.479$ Mc.

The case $J = 3$ is also of practical interest (resonance of B^{10}). For $H_0 = 0$ we can easily obtain closed formulas for an arbitrary asymmetry parameter

$$\left. \begin{aligned} \lambda_1 &= -\frac{1}{10} \left(1 + \sqrt{1 + \frac{5}{3} \eta^2} \right), \\ \lambda_2 &= \frac{1-\eta}{20} - \sqrt{\frac{1}{150} (6 + 3\eta + \eta^2)}, \\ \lambda_3 &= \frac{1+\eta}{20} - \sqrt{\frac{1}{150} (6 - 3\eta + \eta^2)}, \\ \lambda_4 &= 0, \\ \lambda_5 &= -\frac{1}{10} \left(1 - \sqrt{1 + \frac{5}{3} \eta^2} \right), \\ \lambda_6 &= \frac{1-\eta}{20} + \sqrt{\frac{1}{150} (6 + 3\eta + \eta^2)}, \\ \lambda_7 &= \frac{1+\eta}{20} + \sqrt{\frac{1}{150} (6 - 3\eta + \eta^2)}. \end{aligned} \right\} \quad (17a)$$

All the energy levels are expressed here in units of eQq_{zz} .

If the spin of the resonating nuclei is $3/2$, then the matrix of the Hamiltonian (10) is written in the form

$$eQq_{zz} \begin{pmatrix} a & e & f & 0 \\ e & c & g & f \\ h & i & d & e \\ 0 & h & e & b \end{pmatrix} \quad (18)$$

with elements

$$\left. \begin{aligned} a &= \frac{1}{4} - \frac{R}{4} \cos \theta, & f &= -\frac{R}{4\sqrt{3}} (\sin \theta \cos \varphi + j \sin \theta \sin \varphi), \\ b &= \frac{1}{4} + \frac{R}{4} \cos \theta, & g &= -\frac{R}{6} (\sin \theta \cos \varphi - j \sin \theta \sin \varphi), \\ c &= -\frac{1}{4} + \frac{R}{12} \cos \theta, & h &= -\frac{R}{4\sqrt{3}} (\sin \theta \cos \varphi - j \sin \theta \sin \varphi), \\ d &= -\frac{1}{4} - \frac{R}{12} \cos \theta, & i &= -\frac{R}{6} (\sin \theta \cos \varphi + j \sin \theta \sin \varphi), \\ e &= \frac{\eta}{4\sqrt{3}}. \end{aligned} \right\} \quad (19)$$

All the rows and columns of the matrix (18) correspond to magnetic quantum numbers $m = +3, -1/2, +1/2$, and $-3/2$. Diagonalization of this matrix for $\theta = 0$ and $\varphi = 0$ makes it possible to obtain in closed form

$$\left. \begin{aligned} \lambda_{1,2} &= \left[\pm \sqrt{\left(\frac{R}{6} - \frac{1}{4}\right)^2 + \frac{\eta^2}{48}} - \frac{R}{12} \right] eQq_{zz}, \\ \lambda_{3,4} &= \left[\pm \sqrt{\left(\frac{R}{6} + \frac{1}{4}\right)^2 + \frac{\eta^2}{48}} + \frac{R}{12} \right] eQq_{zz}. \end{aligned} \right\} \quad (19')$$

Analogously, if $\theta = \pi/2$ and $\varphi = 0$, we get

$$\left. \begin{aligned} \lambda_{1,2} &= \left[\pm \sqrt{\left(\frac{R}{12} + \frac{1}{4}\right)^2 + \frac{(R-\eta)^2}{48}} - \frac{R}{12} \right] eQq_{zz}, \\ \lambda_{3,4} &= \left[\pm \sqrt{\left(\frac{R}{12} - \frac{1}{4}\right)^2 + \frac{(R+\eta)^2}{48}} + \frac{R}{12} \right] eQq_{zz}. \end{aligned} \right\} \quad (20)$$

For $\theta = \pi/2$ and $\varphi = \pi/2$ the energy levels will be

$$\left. \begin{aligned} \lambda_{1,2} &= \left[\pm \sqrt{\left(\frac{R}{12} + \frac{1}{4}\right)^2 + \frac{(R+\eta)^2}{48}} - \frac{R}{12} \right] eQq_{zz}, \\ \lambda_{3,4} &= \left[\pm \sqrt{\left(\frac{R}{12} - \frac{1}{4}\right)^2 + \frac{(R-\eta)^2}{48}} + \frac{R}{12} \right] eQq_{zz}. \end{aligned} \right\} \quad (21)$$

Thus, we can obtain the exact solution of the problem in six different cases. For the resonance of Na^{23} in $Na_2S_2O_3 \cdot 5H_2O$ we have $eQq_{zz} = 0.8$ Mc and 2.26 Mc, $\eta = 0.334$ (for NSR only the larger quadrupole coupling is of interest; the lower value, which leads to a certain complication of the spectrum, is disregarded). Here, too, we observe crossing of the energy levels in two cases. When $\theta = 0$ and $\varphi = 0$ the crossing is at $R = \sqrt{9 - \eta^2}$, and when $\theta = \pi/2$ and $\varphi = \pi/2$ it occurs at the point $R = \sqrt{2\eta^2 + 6\eta}$ (Fig. 3).

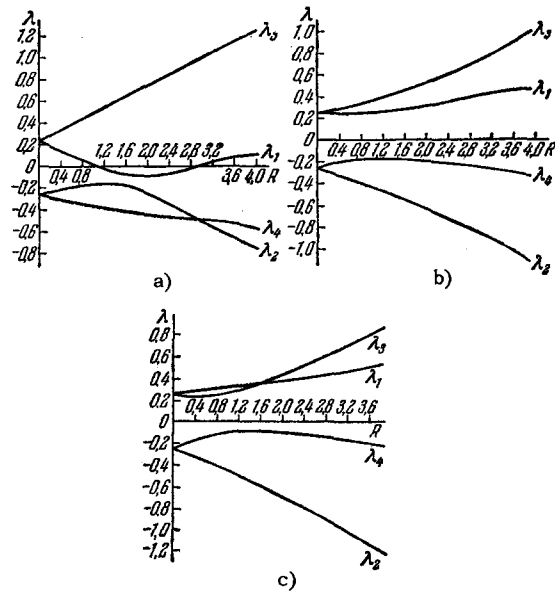


FIG. 3. NSR energy levels in sodium thiosulfate (Na^{23} resonance).
a) $\theta = 0, \varphi = 0$; b) $\theta = \pi/2, \varphi = 0$; c) $\theta = \pi/2, \varphi = \pi/2$

By measuring the absorption frequencies at the points of level crossing we can determine η with a good degree of accuracy, since a unique connection exists between $R(H_0)$ and the asymmetry parameter. We note that the expression for the crossing points does not depend on the magnitude of the nuclear spin.

If $\sin^2 \theta = 2/(3 - \eta \cos 2\varphi)$, then the secular equation for the eigenvalues becomes biquadratic, and therefore

$$\lambda_{1,2,3,4} = \pm eQq_{zz} \times \sqrt{\frac{1}{16} \left(1 + \frac{\eta^2}{3} \right) + \frac{5R^2}{144} \pm \frac{R}{72} \sqrt{4(R^2 + 3\eta^2) + 9(9 - \eta^2) \cos^2 \theta}}. \quad (21a)$$

In this case the energy levels are symmetrical with respect to the abscissa axis, which causes the transition frequency $\nu_{2,1}$ to equal $\nu_{4,3}$ and $\nu_{2,4}$ to equal $\nu_{1,3}$ for arbitrary R. This case is of interest in the production of so-called "negative" temperatures, when the application of the pumping field saturates the transitions $\nu_{2,1}$ and $\nu_{4,3}$ simultaneously so that an excess population of the λ_1 level over λ_4 is obtained. The frequencies of transitions $\nu_{2,1}$ and $\nu_{4,3}$ are the same here, so that the saturating voltage is applied at the frequency $\nu_S = \nu_{2,1} = \nu_{4,3}$.

In the case of arbitrary θ and φ , the energy levels can be readily constructed for specific crystals. We note that the crossing of the level occurs only at the two orientations of H_0 indicated above.

2. NSR Energy Levels for Spin $5/2$

The first numerical calculations of the NSR spectrum for the Al^{27} resonance in $LiAl(SiO_3)_2$ were made in [34]. The calculations were carried out only for the case when $H_0 \parallel Z$. In [9] these calculations were continued and an electronic computer used. The eigenvalues of the Hamiltonian were tabulated for the magnetic field in the XZ plane.

The calculation reduces to diagonalization of the following matrix:

$$eQq_{zz} \begin{pmatrix} a & h & 0 & g & 0 & 0 \\ h & c & j & i & k & 0 \\ 0 & j & e & 0 & i & g \\ g & i & 0 & b & j & 0 \\ 0 & k & i & j & d & h \\ 0 & 0 & g & 0 & h & f \end{pmatrix}, \quad (22)$$

where the rows and the columns correspond to the eigenvectors of the operator I_Z with $m = 5/2, 1/2, -3/2; 3/2, -1/2, -5/2$, and the matrix elements are

$$\left. \begin{aligned} a &= \frac{1}{4} - \frac{R}{4} \cos \theta, & g &= -\frac{R}{4\sqrt{5}} \sin \theta, \\ b &= -\frac{1}{20} - \frac{3R}{20} \cos \theta, & h &= \frac{\eta}{4\sqrt{10}}, \\ c &= -\frac{1}{5} - \frac{R}{20} \cos \theta, & i &= -\frac{\sqrt{2}R}{10} \sin \theta, \\ d &= -\frac{1}{5} + \frac{R}{20} \cos \theta, & j &= \frac{3\eta}{20\sqrt{2}}, \\ e &= -\frac{1}{20} + \frac{3R}{20} \cos \theta, & k &= -\frac{3R}{20} \sin \theta, \\ f &= \frac{1}{4} + \frac{R}{4} \cos \theta, & & \end{aligned} \right\} \quad (23)$$

For spodumene $\eta = 0.93$ and $eQq_{zz} = 2.95$ Mc (Al^{27}). In the calculation, θ was varied from 0 to 90° in steps of 10° and R from 0 to 3.2 in steps of 0.4. Figure 4 shows the energy levels for two values of θ . It is seen from the figure that when $\theta = 0^\circ$ level crossing points are also observed. On the other hand, if $\theta = 10^\circ$ there is no crossing of the levels. The matrices given above make it possible to calculate relatively rapidly the energy levels for specific substances by diagonalizing these matrices. [35]

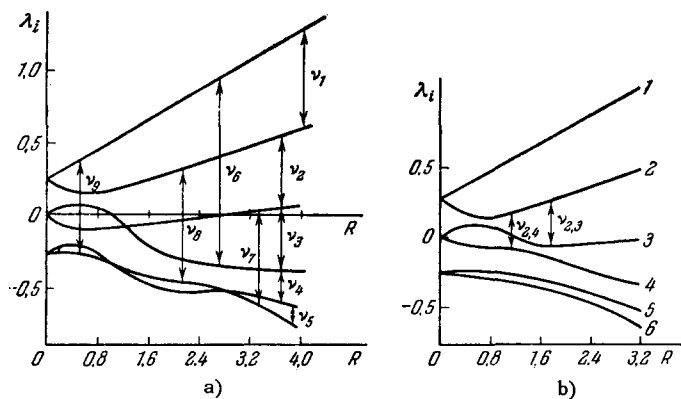


FIG. 4. NSR energy levels in spodumene (resonance of Al^{27}).
a) $\theta = 0^\circ$, b) $\theta = 10^\circ$

III. RELATIVE INTENSITIES OF NSR LINES

1. Relative Intensity of Zeeman Components in NQR

Following the discovery by Kruger [36] of the Zeeman effect in NQR, much research was done on the splitting of the energy levels. The intensity in the absence of axial symmetry of the electric gradient tensor ($\eta \neq 0$) was considered only partially by Dean [24], Cohen [25], and Toyama [37]. The reason for this situation was that intensity calculations were much more complicated than energy-level calculations.

Toyama [37] calculated the relative intensities of the Zeeman spectrum for an arbitrary half-integer spin. Using perturbation theory to second order inclusive, he obtained rather cumbersome expressions for relative line intensities, but valid for arbitrary crystal rotation angles. In the case $J = 3/2$ his expressions are valid (in a weak field H_0) for arbitrary η (Fig. 5). In all other cases, the relations given by

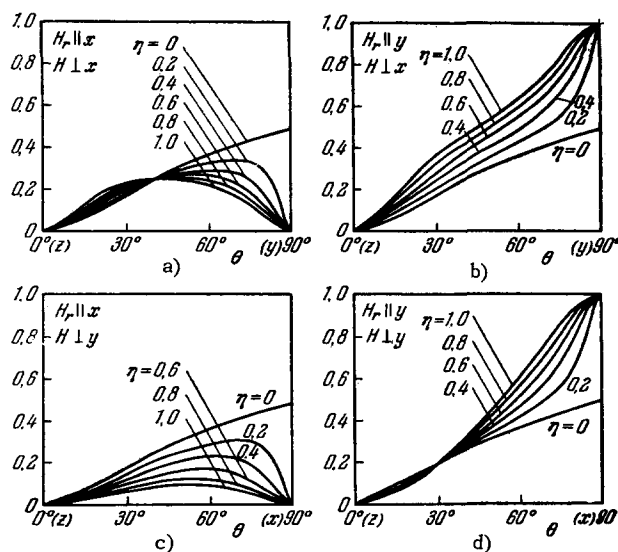


FIG. 5. Relative intensities of the Zeeman components of the NQR spectrum for spin $J = 3/2$.

Toyama hold only when the asymmetry parameter η is small and the spin is not high. In the case of integer spin ($J = 1$) Toyama gives only expressions for the energy levels and the transition intensities, but without indicating the placement of the crystal relative to the constant and alternating fields.

His expressions are: energy levels

$$\begin{cases} E_1 = -2A, \\ E_{2,3} = A \left[1 \pm \left(\eta^2 + \frac{\gamma^2 H^2}{A^2} \right)^{1/2} \right], \end{cases}$$

where $A = \frac{1}{4} e Q q_{zz}$ and γ — gyromagnetic ratio of the nucleus; transition intensities:

$$\begin{cases} \frac{1}{2} \left[1 \pm \left(1 + \frac{\gamma^2 H^2}{\eta^2 A^2} \right)^{-1/2} \right], \\ \left(1 + \frac{\gamma^2 H^2}{\eta^2 A^2} \right)^{-1}. \end{cases}$$

These expressions agree with those obtained in [30,38] (see below) for the particular case when the external constant magnetic field H_0 is directed along the Z axis ($\theta = 0$, $\varphi = 0$), and the alternating field H_r directed along X, Y, and Z, respectively. The dependence of the intensity on the direction of the constant field H_0 in the XZ plane and on the parameter $\gamma H/A\eta$ $\equiv R/\eta$ (in our notation) is also given for $J = 1$. This dependence is shown in Fig. 6. We now proceed to consider results of line intensity calculations which are valid for intermediate magnetic fields.

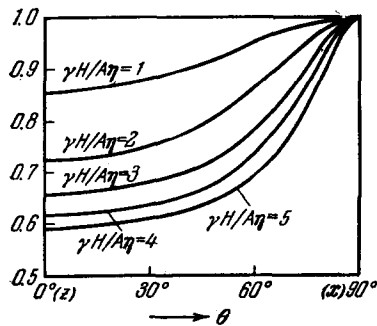


FIG. 6. Dependence of intensity of the transition $\nu_{3,1}$ for $J = 1$ on the direction of the constant magnetic field and the parameter $\gamma H/A\eta$.

2. Generalized NSR Equations

The macroscopic equations of nuclear magnetic resonance were first derived by Bloch [39]. These equations are valid with sufficient degree of accuracy for liquids [40], many phenomena in which can be explained quite lucidly by solving Bloch's equations [41-43].

A generalization of these equations to the case of NSR is found in [9]. Assume that these are two energy levels E_1 and E_2 :

$$\mathcal{H}_0 \psi_1 = E_1 \psi_1, \quad \mathcal{H}_0 \psi_2 = E_2 \psi_2. \quad (24)$$

The perturbation operator (the effect of the radio-frequency field) is written in the form

$$\mathcal{H} = -\gamma \hat{I} H, \quad (25)$$

where γ — gyromagnetic ratio of the nucleus, \hat{I} — mechanical momentum operator of the nucleus, and H — time dependent external radio-frequency field.

We introduce the notation

$$\left. \begin{aligned} (\psi_1^* | I_x | \psi_2) &= (\psi_2^* | I_x | \psi_1) = P, \\ (\psi_1^* | I_y | \psi_2) &= -(\psi_2^* | I_y | \psi_1) = iS, \\ (\psi_1^* | I_z | \psi_2) &= (\psi_2^* | I_z | \psi_1) = T. \end{aligned} \right\} \quad (26)$$

We assume that the solution of the time-dependent Schrödinger equation

$$i\hbar \dot{\psi} = (\mathcal{H}_0 + \mathcal{H}_1) \psi \quad (27)$$

is represented in the form

$$\psi = a\psi_1 + b\psi_2. \quad (28)$$

Substituting (28) in (27) we get

$$\left. \begin{aligned} \dot{a} &= -\left(\frac{iE_1}{\hbar}\right) a - i\gamma (PH_x + TH_z + iSH_y) b, \\ \dot{b} &= -\left(\frac{iE_2}{\hbar}\right) b - i\gamma (PH_x + TH_z - iSH_y) a. \end{aligned} \right\} \quad (29)$$

The mathematical expectation of the mechanical momentum operators will be

$$\left. \begin{aligned} \bar{I}_x(t) &= P(a^*b + b^*a), \\ \bar{I}_y(t) &= iS(a^*b - b^*a). \end{aligned} \right\} \quad (30)$$

On the other hand, the difference in the level populations is given by $n = a^*a - b^*b$. Taking derivatives of $\bar{I}_x(t)$, $\bar{I}_y(t)$ and n and substituting \dot{a} and \dot{b} from (29) we get

$$\left. \begin{aligned} \dot{\bar{I}}_x(t) &= \left(\frac{P}{S}\right) \omega_0 \bar{I}_y(t) - 2\gamma PSH_y n, \\ \dot{\bar{I}}_y(t) &= 2\gamma S(PH_x + PH_z) n - \left(\frac{S}{P}\right) \omega_0 \bar{I}_x(t), \\ \dot{n} &= 2\gamma \left[\left(\frac{S}{P}\right) H_y \bar{I}_x(t) - \frac{(PH_x + TH_z)}{S} \bar{I}_y(t) \right]. \end{aligned} \right\} \quad (31)$$

These equations are analogous to Bloch's equations. Let the radio-frequency field be specified in the form

$$\left. \begin{aligned} H_x &= 2H_1 \sin \theta_1 \cos \varphi_1 \cos \omega t, \\ H_y &= 2H_1 \sin \theta_1 \sin \varphi_1 \cos \omega t, \\ H_z &= 2H_1 \cos \theta_1 \cos \omega t, \end{aligned} \right\} \quad (32)$$

where θ_1 is the angle between the axis of the radio frequency coil and the Z axis, and φ_1 is the azimuth angle. Solving (31), we find that in the single-coil method the absorbed power is proportional to

$$P_a \sim S^2 \sin^2 \theta_1 \sin^2 \varphi_1 + (P \sin \theta_1 \cos \varphi_1 + T \cos \theta_1)^2. \quad (33)$$

Thus, the solution of the generalized NSR equations can be used for line-intensity estimates.

3. Relative Intensities of NSR Lines for Spin 1 or $\frac{3}{2}$

The calculations of the absorption-line intensities for the case of resonating nuclei with spin 1 or $\frac{3}{2}$ were made in [38].

If the eigenvalues of the Hamiltonian (10) are known, then the eigenfunctions are calculated by the usual

Table I. Spin 1

Orientation of constant magnetic field	Energy levels	Wave functions	Orientation of radio-frequency field	Transition	Relative transition intensity
$H_0 \parallel Z$	$\lambda_1 = \frac{1}{4} + \frac{\sqrt{\eta^2 + R^2}}{4}$	$\Psi_1 = C_1\psi_1 + C_2\psi_2$ $C_1 = \frac{\eta}{\sqrt{2(R^2 + \eta^2) + 2R\sqrt{R^2 + \eta^2}}}$ $C_2 = \frac{R + \sqrt{R^2 + \eta^2}}{\sqrt{2(R^2 + \eta^2) + 2R\sqrt{R^2 + \eta^2}}}$	$H_1 \parallel X$	$\nu_{3,1}$	$\frac{1}{2} + \frac{\eta}{2\sqrt{R^2 + \eta^2}}$
	$\lambda_2 = \frac{1}{4} - \frac{\sqrt{R^2 + \eta^2}}{4}$	$\Psi_2 = C'_1\psi_1 + C'_2\psi_2$ $C'_1 = \frac{\eta}{\sqrt{2(R^2 + \eta^2) - 2R\sqrt{R^2 + \eta^2}}}$ $C'_2 = \frac{R - \sqrt{R^2 + \eta^2}}{\sqrt{2(R^2 + \eta^2) - 2R\sqrt{R^2 + \eta^2}}}$		$\nu_{3,2}$	$\frac{1}{2} - \frac{\eta}{2\sqrt{R^2 + \eta^2}}$
	$\lambda_3 = \lambda_2$ when $R = \sqrt{9 - \eta^2}$			$\nu_{3,1}$	$\frac{1}{2} - \frac{\eta}{2\sqrt{R^2 + \eta^2}}$
$H_0 \parallel X$	$\lambda_3 = -\frac{1}{2}$	$\Psi_3 = \psi_3$	$H_1 \parallel Z$	$\nu_{2,1}$	$\frac{\eta^2}{R^2 + \eta^2}$
	$\lambda_1 = -\frac{1 - \eta}{8} + \frac{1}{8}\sqrt{(3 + \eta)^2 + 4R^2}$	$\Psi_1 = C_1\psi_1 + C_2\psi_2 + C_3\psi_3$ $C_1 = C_2 = \frac{(3 + \eta) + \sqrt{(3 + \eta)^2 + 4R^2}}{2\sqrt{(3 + \eta)^2 + 4R^2} + (3 + \eta)\sqrt{(3 + \eta)^2 + 4R^2}}$ $C_3 = -\frac{\sqrt{2}R}{\sqrt{(3 + \eta)^2 + 4R^2} + (3 + \eta)\sqrt{(3 + \eta)^2 + 4R^2}}$		$H_1 \parallel X$	$\nu_{2,1}$
$H_0 \parallel X$	$\lambda_2 = -\frac{1 - \eta}{8} - \frac{1}{8}\sqrt{(3 + \eta)^2 + 4R^2}$	$\Psi_2 = C'_1\psi_1 + C'_2\psi_2 + C'_3\psi_3$ $C'_1 = C'_2 = \frac{(3 + \eta) - \sqrt{(3 + \eta)^2 + 4R^2}}{2\sqrt{(3 + \eta)^2 + 4R^2} - (3 + \eta)\sqrt{(3 + \eta)^2 + 4R^2}}$ $C'_3 = -\frac{\sqrt{2}R}{\sqrt{(3 + \eta)^2 + 4R^2} - (3 + \eta)\sqrt{(3 + \eta)^2 + 4R^2}}$	$H_1 \parallel Y$	$\nu_{2,3}$	$\frac{2R^2}{(3 + \eta)^2 + 4R^2 - (3 + \eta)\sqrt{(3 + \eta)^2 + 4R^2}}$
	$\lambda_3 = \frac{1}{4} - \frac{\eta}{4}$	$\Psi_3 = \frac{1}{\sqrt{2}}\psi_1 - \frac{1}{\sqrt{2}}\psi_2$		$\nu_{3,1}$	$\frac{2R^2}{(3 + \eta)^2 + 4R^2 + (3 + \eta)\sqrt{(3 + \eta)^2 + 4R^2}}$
$H_0 \parallel Y$	$\lambda_1 = -\frac{1 + \eta}{8} + \frac{1}{8}\sqrt{(3 + \eta)^2 + 4R^2}$	$\Psi_1 = C_1\psi_1 + C_2\psi_2 + iC_3\psi_3$ $C_1 = -C_2 = -\frac{(3 - \eta) + \sqrt{(3 - \eta)^2 + 4R^2}}{2\sqrt{(3 - \eta)^2 + 4R^2} + (3 - \eta)\sqrt{(3 - \eta)^2 + 4R^2}}$ $C_3 = -\frac{\sqrt{2}R}{\sqrt{(3 - \eta)^2 + 4R^2} + (3 - \eta)\sqrt{(3 - \eta)^2 + 4R^2}}$	$H_1 \parallel X$	$\nu_{2,3}$	$\frac{2R^2}{(3 - \eta)^2 + 4R^2 - (3 - \eta)\sqrt{(3 - \eta)^2 + 4R^2}}$
	$\lambda_2 = -\frac{1 + \eta}{8} - \frac{1}{8}\sqrt{(3 - \eta)^2 + 4R^2}$	$\Psi_2 = C'_1\psi_1 + C'_2\psi_2 + iC'_3\psi_3$ $C'_1 = -C'_2 = -\frac{(3 - \eta) - \sqrt{(3 - \eta)^2 + 4R^2}}{2\sqrt{(3 - \eta)^2 + 4R^2} - (3 - \eta)\sqrt{(3 - \eta)^2 + 4R^2}}$ $C'_3 = -\frac{\sqrt{2}R}{\sqrt{(3 - \eta)^2 + 4R^2} - (3 - \eta)\sqrt{(3 - \eta)^2 + 4R^2}}$		$\nu_{1,3}$	$\frac{2R^2}{(3 - \eta)^2 + 4R^2 + (3 - \eta)\sqrt{(3 - \eta)^2 + 4R^2}}$
	$\lambda_3 = \frac{1}{4} + \frac{\eta}{4}$	$\Psi_3 = \frac{1}{\sqrt{2}}\psi_1 + \frac{1}{\sqrt{2}}\psi_2$		$\nu_{2,1}$	$\frac{(3 - \eta)^2}{(3 - \eta)^2 + 4R^2}$
	$\lambda_1 = \lambda_3$ when $R = \sqrt{2\eta^2 + 6\eta}$			$\nu_{2,3}$	$\frac{2R^2}{(3 - \eta)^2 + 4R^2 + (3 - \eta)\sqrt{(3 - \eta)^2 + 4R^2}}$
			$\nu_{1,3}$	$\frac{2R^2}{(3 - \eta)^2 + 4R^2 - (3 - \eta)\sqrt{(3 - \eta)^2 + 4R^2}}$	

method^[31]. We consider first the results for spin 1.

For $\theta = 0$ and $\varphi = 0$ (magnetic field directed along the principal axis Z of the electric field gradient tensor) we can obtain after some manipulations

$$\left. \begin{aligned} \Psi_1 &= C_1 \psi_1 + C_2 \psi_2, \\ \lambda_1 &= \frac{1}{4} + \frac{1}{4} \sqrt{R^2 + \eta^2}, \end{aligned} \right\} \quad (34)$$

where

$$\left. \begin{aligned} C_1 &= \frac{\eta}{\sqrt{2(R^2 + \eta^2) + 2R\sqrt{R^2 + \eta^2}}}, \\ C_2 &= \frac{R + \sqrt{R^2 + \eta^2}}{\sqrt{2(R^2 + \eta^2) + 2R\sqrt{R^2 + \eta^2}}}; \\ \Psi_2 &= C'_1 \psi_1 + C'_2 \psi_2, \\ \lambda_2 &= \frac{1}{4} - \frac{1}{4} \sqrt{\eta^2 + R^2}, \end{aligned} \right\} \quad (35)$$

where

$$\left. \begin{aligned} C'_1 &= \frac{\eta}{\sqrt{2(R^2 + \eta^2) - 2R\sqrt{R^2 + \eta^2}}}, \\ C'_2 &= \frac{R - \sqrt{R^2 + \eta^2}}{\sqrt{2(R^2 + \eta^2) - 2R\sqrt{R^2 + \eta^2}}}; \\ \Psi_3 &= \psi_3, \quad \lambda_3 = -\frac{1}{2}. \end{aligned} \right\} \quad (36)$$

Here Ψ_i — orthonormalized eigenfunctions of the unperturbed Hamiltonian, corresponding to eigenvalues λ_i , while ψ_i — orthonormalized eigenfunctions of the operator I_z . If the axis of the radio-frequency coil is directed along X, then $\theta_1 = \pi/2$, $\varphi_1 = 0$, and the absorption is proportional to P.

Let us consider the transition from the level λ_3 to the level λ_1 :

$$P_{3,1} = (0 \ 0 \ 1) \begin{pmatrix} 0 & 0 & \frac{1}{\sqrt{2}} \\ 0 & 0 & \frac{1}{\sqrt{2}} \\ \frac{1}{\sqrt{2}} & \frac{1}{\sqrt{2}} & 0 \end{pmatrix} \begin{pmatrix} C_1 \\ C_2 \\ 0 \end{pmatrix}. \quad (37)$$

Hence

$$P_{3,1}^2 = \frac{1}{2} + \frac{\eta}{2\sqrt{R^2 + \eta^2}}. \quad (38)$$

We calculate analogously the transition probabilities for other cases. The results of the calculations, which are listed in Table I, can be used for all single crystals. The numerical calculations for urea are given in Fig. 7. In (a) are shown the relative intensities of the lines excited when $H_1 \perp H_0$, where H_1 is the radio frequency field. Lines 1 and 6 are excited if $H_0 \parallel X$ and $H_1 \parallel Y$, where X, Y, Z — principal axes of the electric field gradient tensor. Lines 1 and 6 correspond in this case to the transitions $\nu_{2,3}$ and $\nu_{1,3}$, respectively. Lines 2 and 5 are excited if $H_0 \parallel Y$, and $H_1 \parallel X$, and correspond to $\nu_{2,3}$ and $\nu_{1,3}$, respectively. On the other hand, if $H_1 \parallel Z$, then line 2 corresponds to $\nu_{1,3}$ and 5 to $\nu_{2,3}$.

Finally, lines 3 and 4 are excited if $H_0 \parallel Z$ and $H_1 \parallel X$ or $H_1 \parallel Y$. If $H_1 \parallel X$, then line 3 corresponds to $\nu_{3,2}$ and 4 to $\nu_{1,3}$. Analogously, when $H_1 \parallel Y$ line 3 pertains to $\nu_{3,2}$ and 4 to $\nu_{3,1}$.

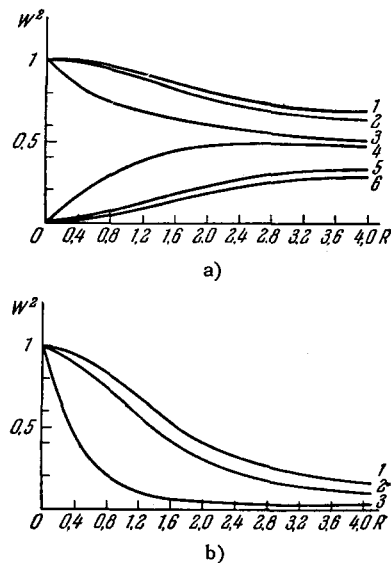


FIG. 7. Relative intensities of NSR lines in urea (resonance of N^{14} nucleus).

a) $H_1 \perp H_0$; b) $H_1 \parallel H_0$.

In (b) are shown the calculated results for parallel fields, when $H_1 \parallel H_0$. In this case line 1 is excited if $H_0 \parallel X$ and corresponds to the transition $\nu_{2,1}$. Analogously, when $H_0 \parallel Y$ line 2 is excited (transition $\nu_{2,1}$), and when $H_0 \parallel Z$ — line 3 (transition $\nu_{2,1}$).

We note that if we exclude the hyperfine structure in the electron paramagnetic resonance spectrum, then the Hamiltonian (10), with suitable constants, coincides with the spin Hamiltonian^[44]

$$\mathcal{H}_{e1} = \frac{D}{3} [3\hat{S}_z^2 - S(S+1)] + \frac{E}{2} (\hat{S}_+^2 + \hat{S}_-^2) - g_e \beta_e \bar{H} \bar{S}, \quad (39)$$

where D — spin Hamiltonian constant describing the level splitting in a zero magnetic field H_0 in the absence of nuclear interaction, \hat{S} — electron spin operator, E — spin Hamiltonian constant, which determines the deviation from the trigonal or tetragonal crystal field towards lower symmetry, g_e — gyromagnetic factor of the electron, and β_e — Bohr magneton.

If we put

$$D = \frac{3}{4} \frac{eQq_{zz}}{S(2S-1)} \quad \text{and} \quad E = \frac{eQq_{zz}}{4S(2S-1)} \eta,$$

then the formulas obtained can be readily rewritten for the case of electron paramagnetic resonance. In place of R we simply put

$$R = \frac{3g_e \beta_e H_0}{D(2S-1)},$$

where S is the effective electron spin, and $\eta = 3E/D$. In this case the electron paramagnetic resonance levels will be expressed in units of $\frac{4}{3} DS(2S-1)$.

The results of the analytical calculations for spin $\frac{3}{2}$ are listed in Table II. This table is illustrated with figures 8–10. Figure 8 shows the dependence of the NSR line intensity of Na^{23} in $Na_2S_2O_3 \cdot 5H_2O$ on R

calculated for the case when the constant magnetic field is oriented along Z, while the axis of the radio-frequency coil is oriented along X, Y, or Z (Figs. 8a, b, and c, respectively). Strong interference of the intensities is observed at $R = 1.5$. In the case of Fig. 8a, the intensity of the line $\nu_{1,4}$ reaches in this region a maximum value, while the integral intensity of the line $\nu_{2,4}$ drops to zero. In the case of Fig. 8b, on the other hand, it is the intensity of $\nu_{4,1}$

which drops to zero, while $\nu_{2,4}$ has a maximum intensity. Another case of interest is that of parallel fields $H_1 \parallel H_0 \parallel Z$ (see Fig. 8c), where a sharp maximum in the intensity of the transition $\nu_{2,1}$ is observed (the absorption increases by a factor of approximately 30). This feature of the spectrum is manifest in the region of the "gap" between the energy levels, which may be of interest for acoustic resonance^[81]. The position of the maximum of the intensity of the $\nu_{2,1}$ transition

Table II. Spin $\frac{3}{2}$

Orientation of constant magnetic field	Energy levels	Wave functions	Orientation of radio-frequency field	Transition	Relative transition intensity
$H_0 \parallel Z$	$\lambda_1 = \sqrt{\left(\frac{R}{6} - \frac{1}{4}\right)^2 + \frac{\eta^2}{48}} - \frac{R}{12}$	$\Psi_1 = C_1\psi_1 + C_2\psi_2$ $C_1 = \frac{1}{\sqrt{2}} \sqrt{1 - \frac{b_-}{a_-}} \equiv \alpha_-$ $C_2 = \frac{1}{\sqrt{2}} \sqrt{1 + \frac{b_-}{a_-}} \equiv \beta_-$ $a_{\pm} = \sqrt{\left(\frac{R}{6} \pm \frac{1}{4}\right)^2 + \frac{\eta^2}{48}}$ $b_{\pm} = \left(\frac{R}{6} \pm \frac{1}{4}\right)$	$H_1 \parallel X$	$\nu_{1,3}$	$\left[\left(\frac{\sqrt{3}}{2} \alpha_- + \beta_- \right) \alpha_+ + \frac{\sqrt{3}}{2} \beta_- \beta_+ \right]^2$
	$\lambda_2 = -\sqrt{\left(\frac{R}{6} - \frac{1}{4}\right)^2 + \frac{\eta^2}{48}} - \frac{R}{12}$	$\Psi_2 = C'_1\psi_1 + C'_2\psi_2$ $C'_1 = C_2, C'_2 = -C_1$ $\Psi_3 = C_3\psi_3 + C_4\psi_4$ $C_3 = \frac{1}{\sqrt{2}} \sqrt{1 - \frac{b_+}{a_+}} \equiv \alpha_+$ $C_4 = \frac{1}{\sqrt{2}} \sqrt{1 + \frac{b_+}{a_+}} \equiv \beta_+$		$\nu_{4,1}$	$\left[\frac{\sqrt{3}}{2} \beta_+ \alpha_- + \left(\beta_+ - \frac{\sqrt{3}}{2} \alpha_+ \right) \beta_- \right]^2$
	$\lambda_3 = \sqrt{\left(\frac{R}{6} + \frac{1}{4}\right)^2 + \frac{\eta^2}{48}} + \frac{R}{12}$	$\Psi_4 = C_3\psi_3 + C_4\psi_4$ $C_3 = C_4, C_4 = -C_3$		$\nu_{2,3}$	$\left[\left(\frac{\sqrt{3}}{2} \beta_- - \alpha_- \right) \alpha_+ - \frac{\sqrt{3}}{2} \alpha_- \beta_+ \right]^2$
	$\lambda_4 = -\sqrt{\left(\frac{R}{6} + \frac{1}{4}\right)^2 + \frac{\eta^2}{48}} + \frac{R}{12}$			$\nu_{2,4}$	$\left[\left(\frac{\sqrt{3}}{2} \beta_- - \alpha_- \right) \beta_+ + \frac{\sqrt{3}}{2} \alpha_- \alpha_+ \right]^2$
$\lambda_2 = \lambda_4$ when $R = \sqrt{9 - \eta^2}$			$H_1 \parallel Y$	$\nu_{1,3}$	$\left[\left(\frac{\sqrt{3}}{2} \alpha_- - \beta_- \right) \alpha_+ + \frac{\sqrt{3}}{2} \beta_- \beta_+ \right]^2$
$H_0 \parallel X$	$\lambda_{1,2} = \pm \sqrt{\left(\frac{R}{12} + \frac{1}{4}\right)^2 + \frac{(R-\eta)^2}{48}} - \frac{R}{12}$	$\Psi_{1,2} = C_1^{(1,2)}\psi_1 + C_2^{(1,2)}\psi_2 + C_3^{(1,2)}\psi_3 + C_4^{(1,2)}\psi_4$ $C_1^{(1,2)} = \frac{R-\eta}{\sqrt{2 \left[(R-\eta)^2 + \left(\frac{1}{4} - \lambda_{1,2}\right)^2 \cdot 48 \right]}}$ $C_2^{(1,2)} = \frac{\left(\frac{1}{4} - \lambda_{1,2}\right) 4\sqrt{3}}{\sqrt{2 \left[(R-\eta)^2 + \left(\frac{1}{4} - \lambda_{1,2}\right)^2 \cdot 48 \right]}}$	$H_1 \parallel X$	$\nu_{2,1}$	$\left[\sqrt{3} C_2^{(1)} C_1^{(2)} + 2 \left(C_2^{(1)} + \frac{\sqrt{3}}{2} C_1^{(1)} \right) C_2^{(2)} \right]^2$
	$\lambda_{3,4} = \pm \sqrt{\left(\frac{R}{12} - \frac{1}{4}\right)^2 + \frac{(R+\eta)^2}{48}} + \frac{R}{12}$	$\Psi_{3,4} = C_1^{(3,4)}\psi_1 + C_2^{(3,4)}\psi_2 - C_3^{(3,4)}\psi_3 - C_4^{(3,4)}\psi_4$ $C_1^{(3,4)} = \frac{R+\eta}{\sqrt{2 \left[(R+\eta)^2 + \left(\frac{1}{4} - \lambda_{3,4}\right)^2 \cdot 48 \right]}}$ $C_2^{(3,4)} = -\frac{4\sqrt{3} \left(\frac{1}{4} - \lambda_{3,4}\right)}{\sqrt{2 \left[(R+\eta)^2 + \left(\frac{1}{4} - \lambda_{3,4}\right)^2 \cdot 48 \right]}}$		$\nu_{4,3}$	$\left[\sqrt{3} C_2^{(3)} C_1^{(4)} + 2 C_2^{(4)} \left(C_2^{(3)} + \frac{\sqrt{3}}{2} C_1^{(3)} \right) \right]^2$
				$\nu_{1,3}$	$\left[\sqrt{3} C_2^{(1)} C_1^{(3)} + 2 \left(\frac{\sqrt{3}}{2} C_1^{(1)} - C_2^{(1)} \right) C_2^{(3)} \right]^2$
				$\nu_{4,1}$	$\left[\sqrt{3} C_2^{(1)} C_1^{(4)} + 2 \left(\frac{\sqrt{3}}{2} C_1^{(1)} - C_2^{(1)} \right) C_2^{(4)} \right]^2$
			$H_1 \parallel Y$	$\nu_{2,3}$	$\left[\sqrt{3} C_2^{(2)} C_1^{(3)} + 2 \left(\frac{\sqrt{3}}{2} C_1^{(2)} - C_2^{(2)} \right) C_2^{(3)} \right]^2$
			$H_1 \parallel Z$	$\nu_{2,4}$	$\left[\sqrt{3} C_2^{(2)} C_1^{(4)} + 2 \left(\frac{\sqrt{3}}{2} C_1^{(2)} - C_2^{(2)} \right) C_2^{(4)} \right]^2$
			$H_1 \parallel Z$	$\nu_{1,3}$	$(3C_1^{(1)}C_1^{(3)} - C_2^{(1)}C_2^{(3)})^2$
			$H_1 \parallel Z$	$\nu_{4,1}$	$(3C_1^{(1)}C_1^{(4)} - C_2^{(1)}C_2^{(4)})^2$
			$H_1 \parallel Z$	$\nu_{2,3}$	$(3C_1^{(2)}C_1^{(3)} - C_2^{(2)}C_2^{(3)})^2$
			$H_1 \parallel Z$	$\nu_{2,4}$	$(3C_1^{(2)}C_1^{(4)} - C_2^{(2)}C_2^{(4)})^2$

Table II. (continued)

Orientation of constant magnetic field	Energy levels	Wave functions	Orientation of radio-frequency field	Transition	Relative transition intensity
$H_0 \parallel Y$	$\lambda_{1,2} = \pm \sqrt{\left(\frac{R-1}{12} + \frac{(R+\eta)^2}{48}\right) - \frac{R}{12}}$	$\Psi_{1,2} = C_1^{(1,2)}\psi_1 + C_2^{(1,2)}\psi_3 + jC_2^{(1,2)}\psi_3 + jC_1^{(1,2)}\psi_4$ $C_1^{(1,2)} = \frac{R+\eta}{\sqrt{2\left[(R+\eta)^2 + \left(\frac{1}{4} - \lambda_{1,2}\right)^2 \cdot 48\right]}}$	$H_1 \parallel X$	$\nu_{1,3}$	$\left[\sqrt{3} C_2^{(1)} C_1^{(3)} + 2 \left(\frac{\sqrt{3}}{2} C_1^{(1)} + C_2^{(1)} \right) C_2^{(3)} \right]^2$
				$\nu_{4,1}$	$\left[\sqrt{3} C_2^{(4)} C_1^{(1)} + 2 \left(\frac{\sqrt{3}}{2} C_1^{(4)} + C_2^{(4)} \right) C_2^{(1)} \right]^2$
	$\lambda_{3,4} = \pm \sqrt{\left(\frac{R-1}{12} + \frac{(R-\eta)^2}{48}\right) + \frac{R}{12}}$ $\lambda_1 = \lambda_3$ when $R = \sqrt{2\eta^2 + 6\eta}$	$\Psi_{3,4} = C_1^{(3,4)}\psi_1 + C_2^{(3,4)}\psi_2 - jC_2^{(3,4)}\psi_3 - jC_1^{(3,4)}\psi_4$ $C_1^{(3,4)} = \frac{R-\eta}{\sqrt{2\left[(R-\eta)^2 + \left(\frac{1}{4} - \lambda_{3,4}\right)^2 \cdot 48\right]}}$	$H_1 \parallel Y$	$\nu_{2,3}$	$\left[\sqrt{3} C_2^{(2)} C_1^{(3)} + 2 \left(\frac{\sqrt{3}}{2} C_1^{(2)} + C_2^{(2)} \right) C_2^{(3)} \right]^2$
				$\nu_{2,4}$	$\left[\sqrt{3} C_2^{(2)} C_1^{(4)} + 2 \left(\frac{\sqrt{3}}{2} C_1^{(2)} + C_2^{(2)} \right) C_2^{(4)} \right]^2$
$H_0 \parallel Z$	$\lambda_{1,2} = \pm \sqrt{\left(\frac{R-1}{12} + \frac{(R+\eta)^2}{48}\right) - \frac{R}{12}}$	$\Psi_{1,2} = C_1^{(1,2)}\psi_1 + C_2^{(1,2)}\psi_3 + jC_2^{(1,2)}\psi_3 + jC_1^{(1,2)}\psi_4$ $C_1^{(1,2)} = \frac{R+\eta}{\sqrt{2\left[(R+\eta)^2 + \left(\frac{1}{4} - \lambda_{1,2}\right)^2 \cdot 48\right]}}$	$H_1 \parallel X$	$\nu_{2,1}$	$\left[-\sqrt{3} C_2^{(2)} C_1^{(1)} + 2 \left(C_2^{(2)} - \frac{\sqrt{3}}{2} C_1^{(2)} \right) C_2^{(1)} \right]^2$
				$\nu_{4,3}$	$\left[\sqrt{3} C_2^{(4)} C_1^{(3)} + 2 \left(\frac{\sqrt{3}}{2} C_1^{(4)} - C_2^{(4)} \right) C_2^{(3)} \right]^2$
	$\lambda_{3,4} = \pm \sqrt{\left(\frac{R-1}{12} + \frac{(R-\eta)^2}{48}\right) + \frac{R}{12}}$ $\lambda_1 = \lambda_3$ when $R = \sqrt{2\eta^2 + 6\eta}$	$\Psi_{3,4} = C_1^{(3,4)}\psi_1 + C_2^{(3,4)}\psi_2 - jC_2^{(3,4)}\psi_3 - jC_1^{(3,4)}\psi_4$ $C_1^{(3,4)} = \frac{R-\eta}{\sqrt{2\left[(R-\eta)^2 + \left(\frac{1}{4} - \lambda_{3,4}\right)^2 \cdot 48\right]}}$	$H_1 \parallel Y$	$\nu_{1,3}$	$(3C_1^{(1)}C_1^{(3)} - C_2^{(1)}C_2^{(3)})^2$
				$\nu_{4,1}$	$(3C_1^{(4)}C_1^{(1)} - C_2^{(4)}C_2^{(1)})^2$
$H_0 \parallel Z$	$\lambda_{1,2} = \pm \sqrt{\left(\frac{R-1}{12} + \frac{(R+\eta)^2}{48}\right) - \frac{R}{12}}$	$\Psi_{1,2} = C_1^{(1,2)}\psi_1 + C_2^{(1,2)}\psi_3 + jC_2^{(1,2)}\psi_3 + jC_1^{(1,2)}\psi_4$ $C_1^{(1,2)} = \frac{R+\eta}{\sqrt{2\left[(R+\eta)^2 + \left(\frac{1}{4} - \lambda_{1,2}\right)^2 \cdot 48\right]}}$	$H_1 \parallel Z$	$\nu_{2,3}$	$(3C_1^{(2)}C_1^{(3)} - C_2^{(2)}C_2^{(3)})^2$
				$\nu_{2,4}$	$(3C_1^{(2)}C_1^{(4)} - C_2^{(2)}C_2^{(4)})^2$

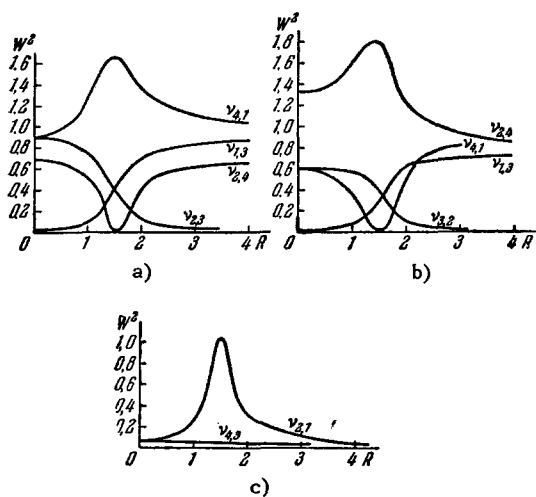


FIG. 8. Relative intensity of NSR lines in thiosulfate (resonance of N_2S , $H_0 \parallel Z$).

a) $H_1 \parallel X$; b) $H_1 \parallel Y$; c) $H_1 \parallel Z$.

does not depend on η , and the maximum occurs for all substances (spin $J = 3/2$) at $R = 3/2$. Then

$$\frac{4\mu H_0}{eQq_{zz}} = \frac{3}{2},$$

and it is possible to determine the quadrupole coupling constant from the value of the field H_0 at which the maximum intensity occurs. On the other hand, the width of the maximum at half the intensity is rig-

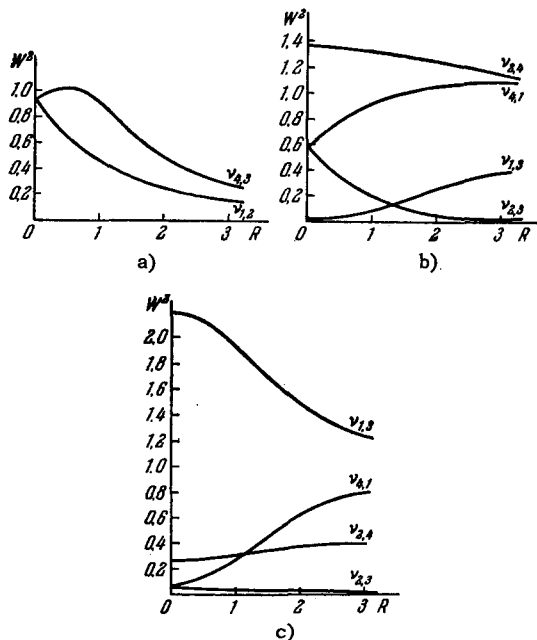


FIG. 9. Relative intensities of NSR lines in sodium thiosulfate ($H_0 \parallel X$).

a) $H_1 \parallel X$; b) $H_1 \parallel Y$; c) $H_1 \parallel Z$.

ously equal to $\sqrt{3}\eta$. Figure 9 shows the line intensity in the case when the constant magnetic field is parallel to X, and the linearly polarized field H_1 is parallel to X, Y, or Z (see Figs. 9a, b, and c, re-

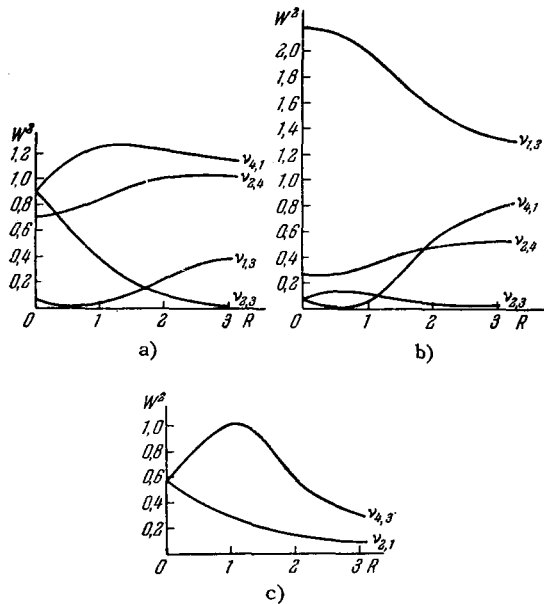


FIG. 10. Relative intensity of NSR lines in $\text{Na}_2\text{S}_2\text{O}_3 \cdot 5\text{H}_2\text{O}$ ($H_0 \parallel Y$).
 a) $H_1 \parallel X$; b) $H_1 \parallel Z$; c) $H_1 \parallel Y$.

spectively). In the case when $H_0 \perp H_1$, four transitions are also observed, and when $H_0 \parallel H_1$, the intensity of the two other transitions differs from zero.

An analogous situation occurs when H_0 is parallel to Y (Fig. 10).

4. Relative Intensities of NSR Lines for Spin $5/2$

The relative intensities of the NSR lines for spin $5/2$ in spodumene were calculated in [45]. Two cases were considered:

- 1) H_1 is linearly polarized along the X axis for arbitrary value of H_0 directed along the Z axis;
- 2) H_1 is linearly polarized along an arbitrary direction relative to the principal axes for the case $H_0 = 0$.

The linearly polarized field H_1 can be resolved into two circularly polarized fields that rotate in opposite directions [39]. In the case of sufficiently large values of H_0 , magnetic interactions predominate, and the quadrupole interaction is only a small perturba-

tion. In this case, therefore, the only effective component of H_1 is the one rotating in the same direction as the Larmor precession of the nuclei. On the other hand, in weak fields, both circularly polarized components of H_1 are important. The authors of [45] have therefore calculated the doubled eigenvalues of the operators. We note that this is not essential in principle, since it is the relative integral line intensities that are calculated. The results of the calculations for spodumene are shown in Fig. 11. A strong interference in the intensities of transitions ν_2 and ν_3 is observed near $R = 0.8$.

Analogous results for $H_0 = 0$ are shown in Table III.

The levels are numbered here in order of increasing energy, and the corresponding transition frequencies are

$$\begin{aligned} \nu_2 = \nu_6 &= 0.789 \text{ Mc } (W_{1\leftrightarrow 2}), \\ \nu_4 = \nu_7 &= 0.758 \text{ Mc } (W_{2\leftrightarrow 3}), \\ \nu_8 = \nu_9 &= 1.547 \text{ Mc } (W_{1\leftrightarrow 3}). \end{aligned}$$

We note that the energy levels at $H_0 = 0$ are doubly degenerate, so that both direct and crossing transitions are included in the transition probability calculations. As is seen from Table III, the line intensities are approximately double in single crystals than in powders ($H_0 = 0$). Numerical calculations for $J = 5/2$ in zero magnetic field are usually not too complicated, and in addition tables have been prepared for this purpose [25] and can be used for rough estimates of the intensities at different values of the asymmetry parameter. The probability of the "forbidden" transition increases with increasing η [25,46].

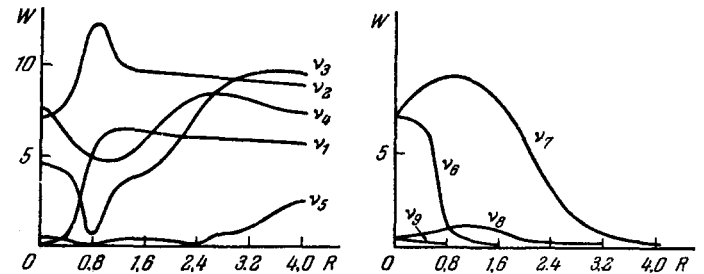


FIG. 11. Relative intensities of Al^{27} lines in spodumene.

Table III

Crystal orientation relative to H_1	Relative Intensities	W	W	W	Crystal orientation relative to H_1	Relative Intensities	W	W	W
		($1\leftrightarrow 2$)	($2\leftrightarrow 3$)	($1\leftrightarrow 3$)			($1\leftrightarrow 2$)	($2\leftrightarrow 3$)	($1\leftrightarrow 3$)
$H_1 \parallel X$	P	7.2	7.5	0.33	$H_1 \parallel Z$	S	0.5	2.6	0.18
$H_1 \parallel Y$	Q	2.8	0.6	0.19	Poly-crystal	$\frac{1}{3}$ (P+ +Q+ +S)	3.5	3.6	0.23

IV. TEMPERATURE DEPENDENCE OF THE ABSORPTION FREQUENCIES AND THEORY OF NUCLEAR SPIN-LATTICE RELAXATION

The first theory of the temperature dependence of the quadrupole coupling constants was developed by Bayer^[57], who took into account the rotational nuclear swings that lead to averaging of the electric field gradient. Bayer, however, took into account only one axis of the rotational swings of the molecules in the crystal. Skripov^[58] constructed a more general theory for the temperature dependence of the NQR frequencies:

1) Since Bayer considered only one particular case of the rotational swing axis OA perpendicular to the electric field symmetry axis OX, more general formulas were obtained, suitable for any direction of OA, and also for the case when the molecule participates simultaneously in several vibrational motions.

2) The calculations were extended to include also small deviations from axial symmetry of the electric field near the nucleus.

3) An approximate calculation was made of the effect of anharmonicity of the rotational swings on the magnitude of the temperature variation.

4) It has been shown that the acoustic vibrations introduce a noticeable contribution to the temperature dependence of the quadrupole resonance frequencies, which for transverse waves can approximately be expressed by the formula

$$\nu(T) - \nu_0 = -\frac{4\pi}{3} \frac{k^4}{h^3} \nu_Q \frac{\theta_D^3}{QC_t^3} TD \left(\frac{\theta_D}{T} \right), \quad (40)$$

where ν_0 — NQR frequency at 0°K, ν_Q — NQR frequency in the absence of lattice vibrations, ρ — crystal density, C_t — speed of transverse acoustic waves, h — Planck's constant, k — Boltzmann's constant, T — absolute temperature, θ_D — characteristic Debye temperature, D — Debye function.

It is seen from (40) that the NQR frequency decreases with rising temperature. This is essentially true for molecular crystals, but for other compounds the temperature coefficient frequently has the opposite sign, i.e., the resonance frequency increases with rising temperature. Bayer's theory, which does not take volume effects into account, is incapable of explaining the positive temperature coefficient. An account of volume effects was given in^[59].

An example of a positive temperature coefficient is afforded by the dependence of the quadrupole coupling constant of Al^{27} on the temperature in four alums, taken from^[87a] (Fig. 12). In nuclear resonance it is customary to consider two relaxation times — transverse and longitudinal. The transverse relaxation time T_2 is a measure of the line width, while the longitudinal or spin-lattice relaxation time T_1 characterizes the rate of establishment of Boltzmann equilibrium. These main characteristics of

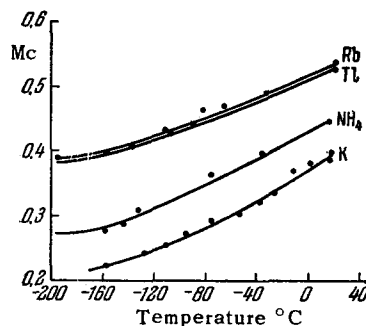


FIG. 12. Temperature dependence of eQq_{zz} of Al^{27} nuclei in single crystals of $MAI(SO_4)_2 \cdot 12H_2O$, where $M = K, NH_4, Tl, Rb$.

spin-lattice and spin-spin relaxation appear also in the presence of the quadrupole relaxation mechanism. The first proof of the reality of the quadrupole mechanism in many crystals was presented by Pound^[1]. He has shown qualitatively that T_1 for the resonance of I^{127} in KI is much smaller than T_1 for the resonance of Na^{23} in $NaNO_3$, which in turn is much smaller than T_1 for the Li^7 resonance in $LiNO_3$. The reason is that the quadrupole moment of I^{127} is considerably larger than that of Li^7 whereas that of Na^{23} has an intermediate value.

Further proof was provided by experiments with $NaBr$ crystals. Na^{23} , Br^{79} , and Br^{81} have spin $3/2$; the magnetic moments of these nuclei are almost identical; consequently, any relaxation mechanism due to magnetic interaction should yield approximately the same relaxation time. Actually, however, the relaxation time for Na^{23} turns out to be almost double that for Br^{81} .

In our measurements, the intensity of the Na^{23} NMR signal is, in this crystal, approximately triple the intensity of the Br^{81} signal. Therefore a study of the relaxation processes for Br^{81} entails some difficulties. As already noted, these experiments were made in strong magnetic fields.

A theory of nuclear quadrupole spin-lattice relaxation for spin $3/2$ in zero magnetic field was constructed by Bayer^[57], who took account of the influence of the rotational swings on the time T_1 . Bayer's formulas were generalized in^[60] to include the case of resonating nuclei with spin 1 or $5/2$. If the time T_1 is measured, then the order of magnitude of the average lifetime of a quantum of the rotational swings can be estimated^[61,62].

However, Bayer's theory is not applicable to ionic crystals or when a strong magnetic field is applied. The temperature dependence of the spin-lattice relaxation time for ionic crystals was elucidated by Van Kranendonk^[63] and Chang^[64]. Van Kranendonk's theory deals with nuclei that relax by interaction between the nuclear quadrupole moments and the time-dependent gradient of the electric field. This time dependence is due to the thermal lattice vibrations in

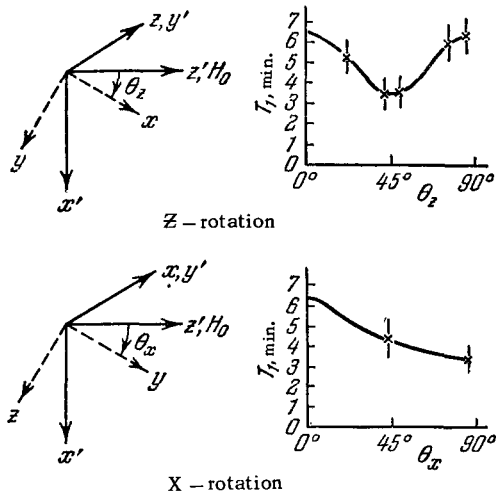


FIG. 13. Dependence of T_1 of deuterons on the orientation of single-crystal KD_2PO_4 in a magnetic field.

Table IV

Crystal	Nucleus	T_1 , sec
LiBr	Br^{79}	0.028
AgBr	Br^{79}	0.016
TlBr	Br^{79}	0.26
KI	I^{127}	0.039

However, theoretical estimates of the absolute values of T_1 are difficult. Van Kranendonk considered only the contribution to the electric field gradient from the nearest ions. For this case he obtained a value of T_1 which was four or six orders of magnitude higher than observed in experiment. Somewhat better agreement with experiment was obtained in [68,69]. In [68] Kondo and Yamashita took into account the influence of the overlap of the atomic wave functions of neighboring ions in alkali-halide crystals. It is known that the overlap integral depends on the distance between ions. In the presence of thermal vibrations of the lattice ions, the degree of wave function overlap will change. Kondo and Yamashita calculated the ratio of the quadrupole relaxation time of the metal nuclei and of the halogen nuclei in the same crystal. The overlap model has yielded satisfactory agreement with the experimental data. An account of the overlap of the wave functions in the crystals has also yielded satisfactory estimates for the chemical shifts, i.e., the difference between resonance frequencies for the given nucleus in the crystal and in the aqueous solution of the same compound.

the crystal. Van Kranendonk's theory is constructed for nuclei in a crystalline electric field with cubic symmetry. It is therefore directly applicable to the case of strong magnetic fields. As reported in [4], Chang's theory is more general. In both the Van Kranendonk and Chang theories the relaxation is due to two-phonon processes (for $T > 1^\circ K$). Both authors have used the Debye distribution for the lattice waves, which is apparently valid only for ionic crystals.

The quadrupole interaction Hamiltonian \mathcal{H}_Q depends on the distances between the given nucleus and the other ions which contribute to the electric field gradient. Therefore, in the presence of lattice oscillations \mathcal{H}_Q can be represented as a function of the small displacements of the ions in the lattice:

$$\mathcal{H}_Q = \mathcal{H}_Q^{(0)} + \mathcal{H}_Q^{(1)} + \mathcal{H}_Q^{(2)} + \dots, \quad (41)$$

where $\mathcal{H}_Q^{(0)}$ does not include the displacements of the ions and is the Hamiltonian of the perturbation of the Zeeman levels in the external magnetic field, while $\mathcal{H}_Q^{(1)}$ includes only those ion displacements whose frequencies lie near the nuclear Larmor precession frequency ω_0 ; on the other hand $\mathcal{H}_Q^{(2)}$ includes the displacements whose difference gives ω_0 , and pertains to the so-called "indirect" relaxation process, which usually predominates. If a Debye distribution with characteristic temperature θ is used for the lattice vibrations, then the temperature dependence of the nuclear spin-lattice relaxation time is

$$\left. \begin{aligned} \frac{1}{T_1} &\sim T^2 \left(a - \frac{b}{T^2} \right) && \text{for } T \gg \frac{1}{2} \theta, \\ \frac{1}{T_1} &\sim T^7 && \text{for } T \leq 0.02\theta, \end{aligned} \right\} \quad (42)$$

where a and b are constants.

Some experimental data on the relaxation time are listed in Table IV, which is taken from [6,65].

It is shown in [69] that if the spin dependence of T_1 is separated, then the ratio of the quadrupole relaxation time T_1 of two isotopes with different spins will be

$$\frac{T_1(J_1)}{T_1(J_2)} = \left(\frac{Q_2}{Q_1} \right)^2 \frac{f(J_1)}{f(J_2)}, \quad (43)$$

where Q_1 and Q_2 are the quadrupole moments of different isotopes of the same nucleus. Since the function $f(J)$ was found to be of the form $(2J+3)/J^2(2J-1)$, a comparison was made with experiment. In particular, the result for the RbCl crystal was

$$\left. \begin{aligned} \left[\frac{Q(Rb^{85})}{Q(Rb^{87})} \right]^2 &= 4.28, && \frac{f(5/2)}{f(3/2)} = 0.24, \\ \frac{T_1(Rb^{87})}{T_1(Rb^{85})} &= 1.027 \text{ theor.}, && \frac{T_1(Rb^{87})}{T_1(Rb^{85})} = 1.23 \text{ expt.} \end{aligned} \right\} \quad (44)$$

The same paper gives measured values of T_1 of I^{127} in crystalline KI between 77 and 800°K. The experimental points fit better the theoretical curve $T_1 \sim T^{-2}$ obtained by considering the two-phonon relaxation process, than the curve $T_1 \sim T^{-4}$ predicted by considering the four-phonon process proposed by Khutsishvili [70].

Recently Hebel and Slichter [71] obtained a relation

between the relaxation time and the probability of the relaxation transition

$$\frac{1}{T_1} = \frac{1}{2} \frac{\sum_{m, \mu} (E_m - E_{m+\mu})^2 W(m, m+\mu)}{\sum_m E_m^2}, \quad (45)$$

where $W(m, m+\mu)$ is the probability of transition of the nucleus from the state m to the state $m+\mu$, while E_m and $E_{m+\mu}$ are the energy levels for these states.

If we substitute for W the expression obtained by Van Kranendonk^[63], we find that T_1 should be isotropic with respect to rotation of the crystal in an external magnetic field. This was experimentally confirmed in^[67] and^[72]. An isotropic value of T_1 of the order of 0.80 ± 0.05 sec was obtained in an InSb single crystal^[67]. The same was approximately obtained for several crystals of CsBr, CsI, and CsCl^[72]. For example, the results obtained for CsBr were $T_1(\text{Cs}) = 1050 \pm 40$ sec and $T_1(\text{Br}) = 0.105 \pm 0.020$ sec.

On the other hand, since the probability of relaxation transition has a strong angular dependence, the relaxation times obviously depend on the orientation of the crystal in the external magnetic field. It is possible that all depends on the magnitude of the external magnetic field and on the nucleus used in the experiment (order of magnitude of the quadrupole coupling constant in the given substance). If the experiments are carried out in strong magnetic fields and in substances with large eQq_{ZZ} , then the transition probability, and consequently also the relaxation time, indeed depend little on the crystal orientation (see Figs. 7–11). On the other hand, if the experiments are made in intermediate fields and with nuclei having small eQq_{ZZ} , then isotropy of the spin-lattice relaxation time T_1 should be observed. Such isotropy was indeed observed^[109]. A series of papers^[73–76] on spin-lattice relaxation in imperfect cubic and non-cubic crystals was published by the Andrew group.

In^[73] a method is given for determining the spin-lattice relaxation mechanism of nuclei. Pound^[1] has already shown that if one of the NMR spectral lines is saturated by a strong radio field, then the signals of the other lines in the spectrum change noticeably when the dominant relaxation mechanism is quadrupole, and do not change when the dominant mechanism is magnetic. The two-coil method of distinguishing between the two mechanisms is not always convenient or suitable, and it is therefore shown in^[73] that a differentiation can be obtained by studying the behavior of the lines for saturation with the single-coil method. Kinetic equations were set up for the energy-level populations of nuclei ($J > \frac{1}{2}$) acted upon by strong constant and radio-frequency magnetic fields. For the case of the stationary state, the solution obtained for the system of kinetic equations is

$$N_m - N_{m'} = \frac{n_0}{1 + \kappa_i p_i}, \quad (46)$$

where the index i pertains to the different excited lines of the spectrum. Here N_m is the population of the level m , n_0 the difference between the level populations in spin-lattice equilibrium, p_i is proportional to the square of the amplitude of the radio-frequency field, and κ_i is a constant.

In the case of the magnetic relaxation mechanism, the value of κ_i was found to be unity for all transitions. On the other hand, for quadrupole relaxation, κ_i had different values for different transitions, as listed in Table I of^[74].

The saturation factor $(1 + \kappa_i p_i)^{-1}$ also differs for each spectral line in the case of the quadrupole relaxation mechanism. Consequently, different radio-frequency power levels are necessary to produce an identical degree of saturation of the different lines. This method served as the basis for the determination of the spin-lattice relaxation mechanism in various single crystals.

Let us present briefly the results obtained in^[74]. A quadrupole spin-lattice relaxation mechanism was found for Na^{23} in synthetic single crystals of NaNO_3 , $\text{Na}_2\text{S}_2\text{O}_3 \cdot 5\text{H}_2\text{O}$, and NaClO_3 in a magnetic field of 6040 Oe at room temperature. The relaxation of Li^7 and Al^{27} in single crystals of the natural mineral spodumene and the relaxation of Al^{27} in the crystal of the euclase mineral were found to be magnetic. It was also observed that the relaxation of B^{11} in a pure synthetic crystal of borax was also magnetic.

It is not surprising that the relaxation mechanism is magnetic in natural single crystals, since they contain a noticeable amount of paramagnetic impurities. Indeed, an estimate of the spin-lattice relaxation time due to these impurities, in accordance with^[70], yields values corresponding to the presence of the same amount of impurities as obtained by a different independent method.

It is indicated in^[74] that the efficiency of the quadrupole relaxation mechanism in ionic crystals is determined, in order of magnitude, by the value of $Q^2(1 - \gamma_\infty)^2$, where Q is the quadrupole moment of the nucleus and γ_∞ is the antiscreening factor.* The value of $Q^2(1 - \gamma_\infty)^2$ is several hundred times smaller in B^{11} than in Na^{23} , so that the magnetic relaxation mechanism for the B^{11} nuclei predominates in the borax crystal.

Some additional information on nuclear spin-lattice relaxation time was obtained by the method of ultrasonic saturation of the levels. Proctor and Robinson^[77,78] used ultrasonic irradiation, at a frequency ω_S , of an NaCl crystal placed in a magnetic field. The

*The antiscreening factor γ_∞ takes into account the distortion of the inner electron shells of the atoms due to the interaction with the quadrupole moment of the nucleus. The antiscreening increases the contribution to the electric field gradient from the charges of the neighboring ions.

difference in the populations between the levels $m = 3/2$ and $m = -3/2$ of Na^{23} was measured against the amplitude of the nuclear induction signal, which followed a short pulse of radio-frequency field of frequency ω_0 equal to the Larmor precession frequency of Na^{23} . When $\omega_s = 2\omega_0$ the ultrasound excited nuclear transitions and the level population difference decreased. Analogous experiments in zero magnetic field were carried out with NaClO_3 by Proctor and Tanttala^[79], who investigated the direct relaxation process. The theory of resonant absorption of ultrasound by paramagnets was first developed by Al'tshuler^[80-82]. This procedure has been named acoustic resonance.

It should be noted that the prediction of this phenomenon by Soviet scientists S. A. Al'tshuler and E. K. Zavoiskii has played a decisive role in its study. The calculation of the paramagnetic sound absorption coefficient is analogous to the calculation of the paramagnetic lattice relaxation time at helium temperatures. On the other hand, the exchange of energy between the spin system and the lattice vibrations is essentially effected, down to helium temperatures, by combination scattering of the phonons. One-phonon processes become essential only at the lowest temperatures.

The development of the acoustic resonance method has opened up new possibilities for the study of spin-lattice relaxation in crystals.

In^[83] the concept of crossing relaxation was introduced. For exactly equidistant levels the Boltzmann distribution over the different spin states is established within a time of the order of T_2 . For non-equidistant levels, the ions in the different states reach equilibrium with the lattice after a time T_1 . When overlap of the resonance lines is possible for approximately equidistant levels, equilibrium is established in some intermediate time, called the crossing relaxation time $T_{2,1}$. The method of Bloembergen and co-workers^[83] consists in taking account of the non-diagonal elements of the spin-spin interaction operator. We note that as R varies it is possible to observe in NSR several regions of crossing relaxation, for example near the points where the levels cross.

V. EXPERIMENTAL PROCEDURE

The experimental procedure in NSR differs somewhat from that used in nuclear magnetic resonance^[7,8]. In NMR the generator-detector frequency is usually not varied over a wide range, since the resonant conditions can be satisfied there by varying the constant magnetic field.

In NSR experiments with a wide range of magnetic fields, it is also necessary to tune the generator frequency. In this sense, the NSR apparatus is similar to the apparatus used in NQR^[3-5]. In NQR, however,

frequency modulation is necessary to observe the spectrum (it is possible to use pulsed Zeeman modulation for polycrystals^[47,48]). In NSR, like in NMR, magnetic modulation is used. The use of magnetic modulation easily eliminates all the difficulties connected with parasitic amplitude modulation when the frequency of the generator-detector deviates.

Inasmuch as NSR lines are usually weak, an automatic recorder is usually employed to register the spectrum^[49], along with a phase detector^[50,51]. Block diagrams of installations of this type have been frequently described in the literature. We note only that in NSR it is possible to employ either the absorption method^[52-54] or the nuclear induction method^[10]. Robinson notes^[10] that the nuclear induction method has made it possible to obtain better sensitivity than the absorption method. Robinson's setup is shown in Fig. 14a.

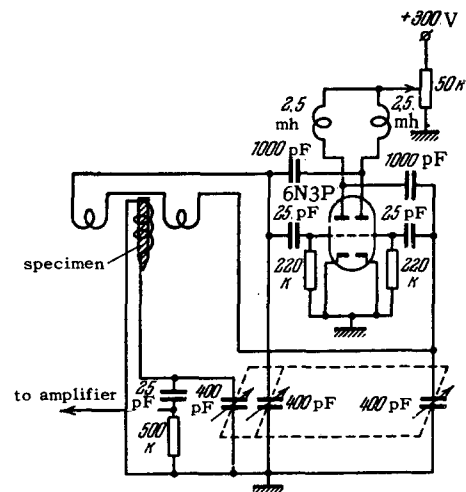


FIG. 14a. Circuit for observation of NSR.

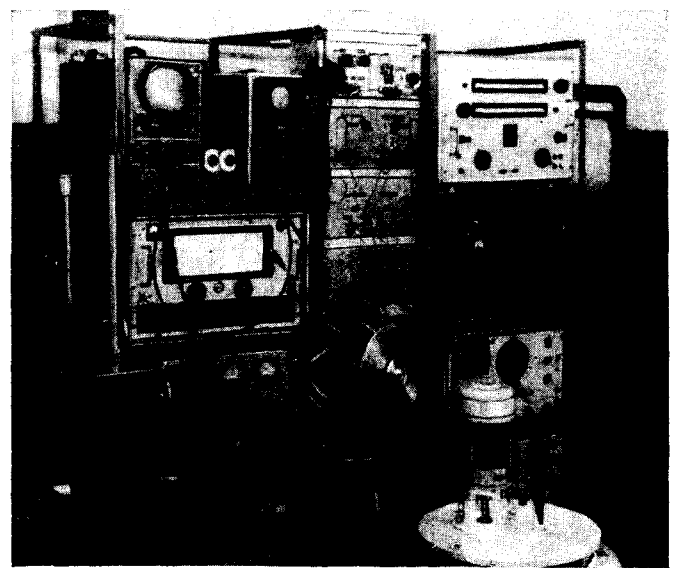


FIG. 14b. Apparatus for observation of NQR.



FIG. 14c. Apparatus for observation of NSR.

Since the use of a radio-frequency bridge decreased the sensitivity by a factor of 5, the nuclear induction method was used. The generator coils had 100 turns each and were wound on a Plexiglas form; the coil inductance was of the order of $250 \mu\text{h}$. Every precaution was exercised to make both halves of the generator coil identical. The specimen was placed in the receiving coil. The crossed coils were then placed in a special copper screen. The magnetic field was modulated with a 225 cps voltage.

Since the experiments were carried out at relatively low frequencies, a sufficient signal/noise ratio could be obtained by using rather large single crystals. Spodumene single crystals weighing 5 and 10 g were used in [10]. A special device made it possible to rotate the crystal inside the receiving coil. Specimens 2.8 cm^3 in volume were also used in [53], and optimum signal amplitude obtained with a radio-frequency coil voltage of 2 V.

A detailed theoretical analysis of the Franklin oscillator circuit (Fig. 15) used in NSR experiments was made by I. M. Ovchinnikov [55], who showed that its circuit is described by fourth-order differential equation and the condition for the self excitation of undamped oscillations in this circuit has the form

$$\frac{2}{R_{a2} C_0 \bar{S}} (C_0 + C) \leq 1, \quad (47)$$

where C_0 is the coupling capacitance between the plate and the grid, C the tank-circuit capacitance, \bar{S} the average tube transconductance and R_{a2} the plate load. The apparatus used in NSR must meet stringent sensitivity requirements. It is sufficient to state that NSR signals of N^{14} in $(\text{CH}_2)_6\text{N}_4$ (Fig. 16a) in a zero

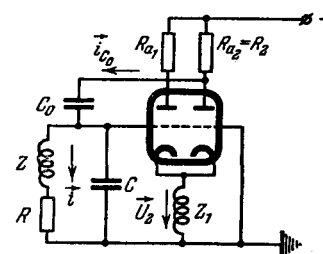
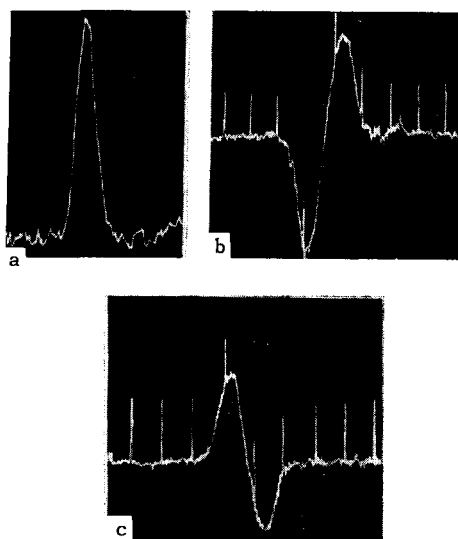


FIG. 15. Diagram of Franklin oscillator.

FIG. 16. a) NSR signal of N^{14} in urotropine; b) Na^{23} signal in NaCl ; c) Na^{23} in NaI .

magnetic field [53] are approximately $1/40$ as weak as the NMR signals on protons in a magnetic field on the order to 2000 Oe in the same compound. In NSR the correct choice of the radio-frequency field level is very important, since it governs the resultant signal/noise ratio. The constant magnetic field is usually produced with electromagnets. Relatively low resolution of the apparatus (on the order of 10^{-6}) is sufficient for this purpose. Rotating magnets of the type described in [52] are very convenient. A convenient magnet gap construction is described in [56]. Although no theory has yet been produced for the NSR line shapes, a study of the line shape becomes essential near the points of level crossing. Consequently superregenerators are not used as a rule for the observation of the signals. In this frequency band the superregenerator distorts the line shape without affording any gain in sensitivity.

VI. EXPERIMENTAL VALUES OF THE QUADRUPOLE INTERACTION CONSTANTS*

Table V lists the experimental values of the quadrupole interaction constants and the asymmetry pa-

*Principal attention is paid to papers published after the reviews [46] and not referred to in [3,5].

Table V. (continued)

Nucleus	Compound	T, °K	Frequency, Mc	eQq_{zz} , Mc	η	Literature source and remarks
N ¹⁴	<i>p</i> -BrC ₆ H ₄ NH ₂	77	2.860			
	HCN	77	3.3417	4.135	0.231	118
		195	2.9178	3.8904	0	121
		77	3.0052	4.0183	0.0085	121
	ClCN	77	3.0223			
			2.400	3.219	0.0137	119
	BrCN	77	2.428			
			2.5109	3.3542	0.006	47, 119
	ICN	199	2.5203	3.4016	0	47
	CH ₃ CN, α -form	77	2.5424			
			2.7992	3.7380	0.0046	120, 129
	CH ₃ CN, β -form	77	2.8078			
			2.7954	3.7375	0.0082	120, 129
	C ₂ H ₅ CN	77	2.8108			
			2.8121	3.7756	0.0208	120, 121, 129
	CH ₂ (CN) ₂	77	2.8513			
			2.8670	3.9216	0.0757	120
	CCL ₃ CN	77	3.0154			
			3.0337	4.0521	0.0053	122
	4-C ₅ H ₄ N(CN)	77	3.0444			
		2.9073	3.8951	0.0144	122	
2-C ₅ H ₄ N(CN)	77	2.9353				
		2.8978	3.9583	0.0716	122	
C ₆ H ₅ (CN)	77	3.0396				
		2.8098	3.8854	0.1073	122	
(CNCl) ₃	77	3.0183				
		3.0445				
Na ²³	NaNO ₃	293	3.0799	4.083	0.017	123
				0.334	0	1, 130; phase transition at 549°K
	NaClO ₃	299	0.3960	0.801	0	124
	NaBrO ₃	293		0.864	0	124
	Na ₂ S ₂ O ₃ ·5H ₂ O	293		2.258	0.334	16
				0.830	0.409	
	NaH ₂ PO ₄ ·2H ₂ O	293		1.179	0.467	125
	NaBF ₄	296		1.09	0	98
	NaAlSi ₃ O ₈ albite	293		2.62	0.25	127
	NaNO ₂	293		1.4003	0.1092	126
Nb ⁹³	KNbO ₃ I	298	3.648 1			129, 131
			3.030 2			
			2.527 3	2.3120	0.806	
			2.085 4			
			2.674 1'			
	KNbO ₃ II	77	2.004 2'			
			1.335 3'			
			0.68 ?			
Rb ⁸⁷	Rb ₂ Mg(SO ₄) ₂ ·6H ₂ O	293		3.141	0.47	102

rameters for several crystals. Only substances in which NSR can be observed are included. The value of eQq_{zz} is chosen such as to make the parameter $R = 4\mu H_0/eQq_{zz}$ not too large for the practically attainable magnetic fields (10–20 kOe). For this purpose it is usually sufficient to have eQq_{zz} of the order of several Mc. In the case of substances with large nuclear magnetic moments (Nb⁹³, Cu⁶³, Cu⁶⁵), quadrupole coupling constants on the order of several times 10 Mc are also suitable for NSR. We shall discuss briefly the experimental results pertaining to the nuclei listed in Table V.

We consider here only questions connected with the NSR energy levels, since knowledge of the quadrupole

interaction constant is decisive in the analysis of the spectrum and the determination of the frequency region and magnetic fields in which this spectrum should be sought.

1) Al²⁷ ($J = 5/2$, $\mu^{27} = 3.6408 \mu_{\text{Nuc}}$). The first to measure the quadrupole coupling constants in aluminum compounds, using the quadrupole splittings of the NMR spectrum, was Pound^[1]. The measurements were made both for powder and for the natural corundum crystal Al₂O₃. The spectrum in a field of 2400 Oe was observed near 3 Mc. The crystal was also rotated and the frequency shift and relative line intensities subsequently measured. However, the small signal/noise ratio did not allow any conclusions to be

drawn concerning the character of the dependence of the intensities on the crystal orientation and the magnitude of the magnetic field. At the present time a systematic study is under way^[15,18-20] of minerals like beryl, chrysoberyl, spodumene, euclase, etc. A detailed study was made^[10] of the resonance of Al^{27} at 660 kcs with $\theta = 0^\circ$ (Fig. 17a) and 800 kcs with $\theta = 5^\circ$ (Fig. 17b). Figure 17c shows the increase in the splitting of the frequencies $\nu_{2,3}$ and $\nu_{2,4}$ at 800 kcs as the angle θ is increased from 0 to 5° . The decrease in the signal amplitude in case (c) is due to the fact that the modulation amplitude is smaller. In cases (a) and (b) the magnetic field is 326 Oe, and in case (c)—369 Oe. Figure 18 shows the experimental and theoretical data. The theoretical continuous curves are in good agreement with the experimental data (see [45]). Deviation from theory is found only for the point of level crossing. For $R = 1.4$, a thorough study of the behavior of the lines has shown that a doublet, not predicted by the theory for $\theta = 0^\circ$, is observed. According to the theory^[9] the levels should cross at this point. Experiment, on the other hand, shows that there is actually no such crossing (see Fig. 17c). The author suggests that this fact can be connected with some weak interaction (which was not taken into account in the calculation of the levels),

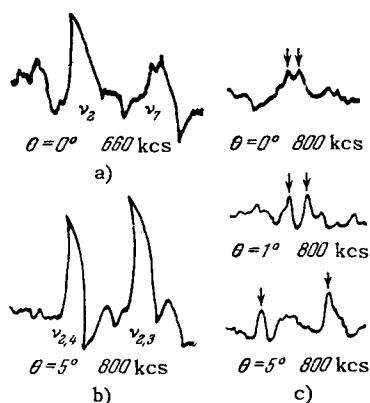


FIG. 17. NSR signals of Al^{27} in spodumene.

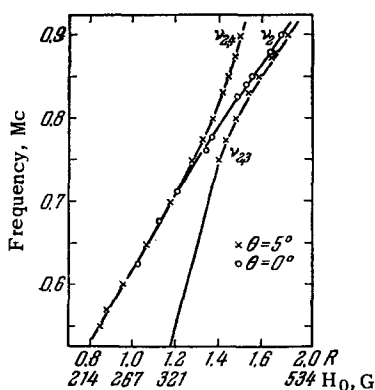


FIG. 18. Comparison of experimental and theoretical results for spodumene. (Resonance of Al^{27}).

leading to the appearance of non-diagonal terms in the Hamiltonian. Such non-diagonal matrix elements can cause changes in the character of the mixing of the wave functions, so that the levels can no longer cross.

It is possible that these are crossing interactions. On the other hand, at $R = 1.4$ a doublet with a splitting on the order of 5 Oe can always be observed in experiment. This doublet could be observed directly at the proposed level crossing point. The observed splitting could be attributed to the fact that the Z axis and the H_0 direction did not coincide, and $\theta = 0.5^\circ$. However, θ was varied in steps of 0.25° and still no point was found at which the doublet would change into a singlet.

2) B^{10} ($J = 3$, $\mu^{10} = 1.8004$) B^{11} ($J = 3/2$, $\mu^{11} = 2.6886$). Petch and co-workers^[94,95] investigated borates (colemanite, inderite, etc). In^[94] the Vol-koff method was used to study resonance in the single crystal of inderite $\text{Mg}_2\text{B}_2\text{O}_{11} \cdot 15\text{H}_2\text{O}$. The measurements were carried out in a field of 7187 Oe at room temperature. By studying the spectrum obtained with the crystal rotated alternately around three mutually perpendicular axes it was concluded that there were three non-equivalent positions in a unit cell with six B^{11} nuclei. The quadrupole coupling constants and the asymmetry parameters were determined (see Table V), as well as the orientations of the principal axes of the electric field gradient tensor for the three indicated positions of the B^{11} nuclei. A comparison was made with the data obtained in^[95] for colemanite $\text{CaB}_3\text{O}_4(\text{OH})_3 \cdot \text{H}_2\text{O}$. Different organic boron compounds have quadrupole coupling constants on the order of 1–5 Mc, i.e., they are suited for investigations in the NSR region. The asymmetry parameters of these compounds are not listed in Table V, since they were investigated^[89,93] without application of a constant magnetic field. Silver and Bray^[96-99] published several papers on the investigation of resonance of P^{31} in different compounds at room temperature. Investigations of B_2O_3 additives in glasses, in a field of 5250 Oe, are reported in^[96]. The dependence of the B^{11} line intensity on the concentrations of these additives was studied. Three nonequivalent positions of B^{11} in the unit cell of the single crystal CB_4 were observed in^[97]. The upper and lower limits of the quadrupole coupling constants were estimated for two positions of B^{11} , and a value $eQq_{zz} = 5.58$ Mc was determined for the third. The asymmetry parameters were found to be equal to zero.

3. Be^9 ($J = 3/2$, $\mu^9 = 1.1774$). The quadrupole coupling constant in metallic beryllium was estimated by Knight^[100]. Using as an example the beryl crystal $\text{Be}_3\text{Al}_2(\text{SiO}_3)_6$, Brown and Williams^[19] developed their already mentioned method of finding the principal axes of the electric field gradient tensor. They plotted the spectra of the beryl single crystal rotated about the principal axes in a field of 7800 Oe at 300°K. The values of the quadrupole coupling constants and asymmetry parameters of the nuclei Be^9 and Al^{27} were found with high accuracy.

4. Cs^{133} ($J = 5/2$, $\mu^{133} = 2.5771$). An estimate of the quadrupole coupling constant was obtained^[102] for only one compound, Tutton's salt $\text{Cs}_2\text{Mg}(\text{SO}_4)_2 \cdot 6\text{H}_2\text{O}$.

5. Cu^{63} ($J = 3/2$, $\mu^{63} = 2.2262$), Cu^{65} ($J = 3/2$, $\mu^{65} = 2.3845$). Inasmuch as the magnetic moment of copper nuclei is relatively large, even substances with large quadrupole coupling constants (10–100 Mc) turn out to be suitable for investigation in the NSR region. Examples are single crystals of cuprous oxide Cu_2O , recently investigated by Cox and Williams^[103]. Earlier measurements with powder have shown that the spectrum lies in the region of 26 Mc for Cu^{63} and 24 Mc for Cu^{65} . On the other hand, work with single crystals has made it possible not only to find with high accuracy the quadrupole coupling constants for the two isotopes (see Table V), but also to determine the directions of the principal axes of the electric field gradient tensor and to estimate the asymmetry parameter. Measurements were also made of the line intensities for different crystal orientations. In a study of single-quantum transitions in fields of 500 and 3000 Oe, it was found that these lines are usually weaker in the stronger fields. On the other hand, the intensity of the line pertaining to the two-quantum transitions increased with increasing H_0 . The behavior of the lines pertaining to the two-quantum transitions was investigated in a field of 2000 Oe as a function of the angle θ . These lines were lost in the noise as θ approached 0° . The spectrum observed near $\theta = 90^\circ$ has several interesting features. As θ approached 90° , the one-quantum and two-quantum lines merged into a single line in a field of 2000 Oe. Another interesting feature was that the line intensities increased more rapidly than expected for $\theta \rightarrow 90^\circ$.

6. D^2 ($J = 1$, $\mu^2 = 0.857348$). Recently an investigation was started^[107-110] of the quadrupole interactions of deuterium nuclei. Of particular interest in this respect is^[109], where single-crystal KD_2PO_4 was investigated. The Volkoff method was used to determine the asymmetry parameters and the quadrupole coupling constant (see Table V). No temperature variations were noted at all in the electric field gradient tensor on going through the ferroelectric Curie point. Neither the quadrupole coupling constant nor the asymmetry parameter changed.

7. K^{39} ($J = 3/2$, $\mu^{39} = 0.391$), K^{41} ($J = 3/2$, $\mu^{41} = 0.215$). The determination of the quadrupole coupling constants of K in potassium chloride is reported by Kaplan and Hahn^[111].

8. Li^6 ($J = 1$, $\mu^6 = 0.82189$), Li^7 ($J = 3/2$, $\mu^7 = 3.2559$). Measurements of the quadrupole coupling constants and of the asymmetry parameters of Li^7 in many compounds were dealt with by Hon and Bray^[112]. The measurements were carried out at room temperature, and eQq_{ZZ} and η were determined from the line splitting in strong magnetic fields.

The spodumene single crystal $\text{LiAl}(\text{SiO}_3)_2$ was investigated by Volkoff's group^[15,51]. It has turned out

that the Y axis of the electric field gradient tensor coincides with the crystallographic b axis (the spodumene single crystal has a monoclinic structure). The other two principal axes lie in the ac plane, and the Z axis, which lies between a and c, makes an angle of $48^\circ \pm 2^\circ$ with the C axis of the crystal.

9. N^{14} ($J = 1$, $\mu^{14} = 0.40365$). The nitrogen nuclei are the most convenient for research in the NSR region, since the quadrupole-coupling constants lie in the 2–4 Mc range. Although the magnetic moment of N^{14} is relatively small, nevertheless at such values of eQq_{ZZ} it is possible to obtain $R \sim 1$ in the feasible fields.

The first successful experiments on NQR in nitrogen were made by Watkins and Pound^[47] as long ago as in 1952. Minematsu^[118] investigated by the Zeeman modulation method single crystals of parabromoaniline, parachloroaniline, parapylenediamine, and urea. The quadrupole coupling constants and asymmetry parameters which she determined are listed in Table V. The directions of the principal axes of the electric field gradient tensor in the single crystal $p\text{-BrC}_6\text{H}_4\text{NH}_2$ were also determined. A group headed by Bray^[110-112] studied systematically the resonances of nitrogen-containing compounds. The structure of these compounds was investigated by a purely quadrupole resonance method.

No NSR experiments have been carried out as yet on N^{14} , so that the calculations in^[30,38] are useful in this respect.

10. Na^{23} ($J = 3/2$, $\mu^{23} = 2.2171$). The first measurements of the quadrupole coupling constant and the asymmetry parameter were made by Pound^[1]. The Itoha method was used in^[16] to obtain the structure of sodium thiosulfate. Two non-equivalent positions of Na^{23} were observed, and eQq_{ZZ} and η were determined for each. In^[30,38] there is a detailed quantum-mechanical calculation of the energy levels and of the relative intensities of the transitions in this single crystal (for the largest quadrupole coupling).

Recently Weiss^[126] experimented with single-crystal NaNO_2 using the Volkoff method. eQq_{ZZ} and η were determined with high accuracy at room temperature.

It was established that the principal axes of the electric field gradient tensor coincided with the orthorhombic crystal axes. The c axis was found to coincide with the direction of the maximum field gradient (i.e., the Z axis). A connection was established between the mosaic structure of the crystal and the width of the nuclear resonance lines with varying angle between the magnetic field H_0 and the principal axes of the electric field gradient tensor of the crystal.

11. Nb^{93} ($J = 9/2$, $\mu^{93} = 6.166$). Cotts and Knight^[129] investigated the nuclear resonance of Nb^{93} in single-crystal KNbO_3 in magnetic fields of the order of 100–5000 Oe and in zero field at temperatures from 77 to 733°K. Phase transitions were detected (from the

changes in the quadrupole splittings of the resonance lines) in strong magnetic fields near 223 and 493°K. KNbO_3 is a ferroelectric with non-cubic crystal structure below the Curie temperature (703°K), becoming cubic above 703°K, with one resonance line observed.

Four lines were observed in zero field at 293°K, and the quadrupole coupling constants and the asymmetry parameter were estimated. The value of the quadrupole coupling constant is compatible with the presence of a strong covalent chemical bond for Nb. The absorption lines were identified and the directions of the principal axes of the electric field gradient tensor of the crystal were determined with the aid of the Zeeman effect in a field of the order of 100 Oe. A recent paper^[131] reports measurements in the temperature region from 4.2 to 693°K and the temperature variations of eQq_{zz} and η are discussed in detail.

12. Rb^{87} ($J = 3/4$, $\mu^{87} = 2.7501$). The quadrupole coupling constant and the asymmetry parameter were measured^[102] for only one compound (Tutton's salt).

We note in conclusion that Table V does not contain many compounds of chlorine, bromine, and iodine, since the quadrupole coupling constants of these nuclei are too large, and therefore the NSR region of interest cannot be obtained in presently feasible magnetic fields*. In addition, these data can be found in^[5].

The NSR method is used successfully for the study of single crystals. Many important results have been obtained for minerals. All this has made it possible to conclude that NSR is a good supplement to the classical method of structural analysis. The particular value of the spin resonance lies in the new possibilities which it uncovers. In particular, it is easy to observe cross relaxation in intermediate fields. Therefore, by equalizing the frequencies for the different groups of nuclei, it is possible to observe signals which are too weak to be experimentally detected under ordinary conditions because the time T_1 is very long. We note that it is frequently impossible to reduce T_1 by other means, since the paramagnetic impurities used for this purpose do not form a solid solution in the specified substance. This is particularly characteristic of aromatic compounds.

Interesting phenomena can be observed in intermediate fields by acoustic resonance, since the transition probabilities in this region depend strongly on the field, often in resonant fashion. As already noted, nuclear spin resonance is a low-frequency model of electron paramagnetic resonance, since the spin Hamiltonians are the same in both cases. Consequently, many phenomena connected with the development of methods for the control of relaxation are easier to study with NSR than with EPR, since broadband os-

cillators are easier to construct for the radio-frequency band. The NSR method is particularly promising in connection with the development of quantum radiophysics, primarily because of its simplicity. The possibility of refining the spin-Hamiltonian constants by checking against the energy level crossing points in intermediate fields is also of considerable interest. Further development of this promising procedure will help solve many problems of scientific and applied character.

¹R. V. Pound, Phys. Rev. **79**, 685 (1950).

²H. G. Dehmelt and H. Krüger, Naturwiss. **37**, 111 (1950).

³V. S. Grechishkin, UFN **69**, 189 (1959), Soviet Phys. Uspekhi **2**, 699 (1960).

⁴T. P. Das and E. L. Hahn, Solid State Phys., Suppl. **1** (1958).

⁵E. I. Fedin and G. K. Semin, ZhSKh (J. of Structural Chemistry) **1** (4), 464 (1960).

⁶M. H. Cohen and F. Reif, Solid State Phys. **5**, 321 (1957).

⁷E. R. Andrew, Nuclear Magnetic Resonance, Cambridge, 1955.

⁸A. Lösche, Kerninduktion, Brl., 1957.

⁹Bloom, Robinson, and Volkoff, Canad. J. Phys. **36**, 1280 (1958).

¹⁰L. B. Robinson, Canad. J. Phys. **36**, 1295 (1958).

¹¹G. M. Volkoff, Canad. J. Phys. **31**, 820 (1953).

¹²Petch, Smellie, and Volkoff, Phys. Rev. **84**, 602 (1951).

¹³R. Bersonn, J. Chem. Phys. **20**, 1505 (1952).

¹⁴Petch, Volkoff, and Cranna, Phys. Rev. **88**, 1201 (1952).

¹⁵Petch, Cranna, and Volkoff, Canad. J. Phys. **31**, 837 (1953).

¹⁶Itoh, Kusaka, and Yamagata, J. Phys. Soc. Japan **9**, 209 (1954).

¹⁷H. H. Waterman and G. M. Volkoff, Canad. J. Phys. **33**, 156 (1955).

¹⁸R. G. Eades, Canad. J. Phys. **33**, 286 (1955).

¹⁹L. C. Brown and D. Williams, J. Chem. Phys. **34**, 751 (1956).

²⁰L. C. Brown and D. Williams, Phys. Rev. **96**, 1110 (1954).

²¹V. V. Lemanov and M. I. Kornfel'd, JETP **39**, 53 (1960), Soviet Phys. JETP **12**, 38 (1960).

²²V. V. Lemanov and M. I. Kornfel'd, JETP **39**, 262 (1960), Soviet Phys. JETP **12**, 188 (1960).

²³V. V. Lemanov, JETP **40**, 775, (1961), Soviet Phys. JETP **13**, 543 (1961).

²⁴C. Dean, Phys. Rev. **96**, 1053 (1954).

²⁵M. H. Cohen, Phys. Rev. **96**, 1278 (1954).

²⁶R. Livingston, Science **118**, 61 (1953).

²⁷Ting, Manring, and Williams, Phys. Rev. **96**, 408 (1954).

²⁸H. Zeldes and R. Livingston, J. Chem. Phys. **26**, 351 (1957).

*Although fields of the order of 10^6 Oe have already been attained, for the observation of NSR it is necessary that such fields be produced in considerable volumes.

- ²⁹ P. M. Parker, *J. Chem. Phys.* **24**, 1096 (1956).
- ³⁰ V. S. Grechishkin and N. E. AĬnbinder, *FTT* **3**, 1821 (1961), *Soviet Phys. Solid State* **3**, 1325 (1961).
- ³¹ L. D. Landau and E. M. Lifshitz, *Quantum Mechanics*, Pergamon, 1958.
- ³² T. C. Wang, *Phys. Rev.* **99**, 566 (1955).
- ³³ Chiba, Toyama, and Morino, *J. Phys. Soc. Japan* **14**, 379 (1959).
- ³⁴ G. Lamarche and G. M. Volkoff, *Canad. J. Phys.* **31**, 1010 (1953).
- ³⁵ V. I. Smirnov, *Kurs vyssheĭ matematiki* (Course of Higher Mathematics) v. 3, part 1, Gostekhizdat, 1949.
- ³⁶ H. Krüger, *Z. Phys.* **130**, 371 (1951).
- ³⁷ M. Toyama, *J. Phys. Soc. Japan* **14**, 1727 (1959).
- ³⁸ V. S. Grechishkin and N. E. AĬnbinder, *FTT* **3**, 2981 (1961), *Soviet Phys. Solid State* **3**, 2175 (1962).
- ³⁹ F. Bloch, *Phys. Rev.* **70**, 460 (1946).
- ⁴⁰ P. M. Borodin, *Dissertation*, Leningrad State Univ. 1955.
- ⁴¹ S. D. Gvozdover and A. A. Magazanik, *JETP* **20**, 705 (1950).
- ⁴² H. C. Torry, *Phys. Rev.* **76**, 1059 (1949).
- ⁴³ V. S. Grechishkin, *JETP* **34**, 902 (1958), *Soviet Phys. JETP* **7**, 625 (1958).
- ⁴⁴ S. A. Al'tshuler and B. M. Kozyrev, *Elektronnyi paramagnitnyi rezonans* (Electron Paramagnetic Resonance), Fizmatgiz, 1961.
- ⁴⁵ G. M. Volkoff and G. Lamarche, *Canad. J. Phys.* **32**, 493 (1954).
- ⁴⁶ R. Braunstein, *Phys. Rev.* **107**, 1195 (1957).
- ⁴⁷ G. D. Watkins and R. V. Pound, *Phys. Rev.* **85**, 1062 (1952).
- ⁴⁸ V. S. Grechishkin, *Vestnik, Leningrad State Univ.* **22**, 19 (1959).
- ⁴⁹ R. V. Pound, *Progr. Nucl. Phys.* **2**, 21 (1952).
- ⁵⁰ N. A. Schuster, *Rev. Scien. Instr.* **22**, 254 (1951).
- ⁵¹ Volkoff, Petch, and Smellie, *Canad. J. Phys.* **30**, 270 (1952).
- ⁵² Aleksandrov, Lundin, and Mikhaĭlov, in coll. "Paramagnitnyi rezonans" (Paramagnetic Resonance), M., 1960.
- ⁵³ V. S. Grechishkin and I. M. Ovchinnikov, *Vestnik, Leningrad State University* **22**, 126 (1960).
- ⁵⁴ V. V. Lemanov, *PTĖ*, No. 1, 126 (1961).
- ⁵⁵ I. M. Ovchinnikov, *Diploma thesis*, Leningrad State Univ., 1960.
- ⁵⁶ N. M. Aleksandrov and V. V. Moskaev, *Vestnik, Leningrad State Univ.* **16**, 14 (1958).
- ⁵⁷ H. Bayer, *Z. Phys.* **130**, 227 (1951).
- ⁵⁸ F. I. Skripov, in coll. "Materialy 10-go Soveschchaniya po spektroskopii" (Proc. 10th Spectroscopy Conf.) v. 1, 1957, p. 76.
- ⁵⁹ Kusnida, Benedek, and Bloembergen, *Phys. Rev.* **104**, 1364 (1956).
- ⁶⁰ V. S. Greshishkin, *FTT* **3**, 1066 (1961), *Soviet Phys. Solid State* **3**, 776 (1961).
- ⁶¹ V. S. Grechishkin and F. I. Skripov, *DAN SSSR* **126**, 1229 (1959), *Soviet Phys. Doklady* **4**, 648 (1959).
- ⁶² V. S. Grechishkin, *Izv. vuzov (Fizika)* (News of the Universities—Physics) No. 5, 11 (1961).
- ⁶³ J. Van Kranendonk, *Physica* **20**, 781 (1954).
- ⁶⁴ C. E. Chang, *Office of Sci. Res. Rep.*, Department Phys., Washington, 1955.
- ⁶⁵ T. Kanda, *J. Phys. Soc. Japan* **10**, 85 (1955).
- ⁶⁶ K. Yosida and T. Moriya, *J. Phys. Soc. Japan* **11**, 33 (1956).
- ⁶⁷ Das, Roy, and Ghosh, *Phys. Rev.* **104**, 1568 (1956).
- ⁶⁸ J. Kondo and J. Yamashita, *J. Phys. Chem. Sol.* **10**, 245 (1959).
- ⁶⁹ R. L. Micher, *Phys. Rev. Letts.* **4**, 57 (1960).
- ⁷⁰ G. R. Khutsishvili, *JETP* **31**, 424 (1956), *Soviet Phys. JETP* **4**, 382 (1956).
- ⁷¹ L. C. Hebel and C. P. Slichter, *Phys. Rev.* **113**, 1504 (1959).
- ⁷² N. Bloembergen and P. P. Sorokin, *Phys. Rev.* **110**, 865 (1958).
- ⁷³ E. R. Andrew and K. M. Swanson, *Proc. Phys. Soc.* **B70**, 476 (1957).
- ⁷⁴ E. R. Andrew and K. M. Swanson, *Proc. Phys. Soc.* **75**, 582 (1960).
- ⁷⁵ Andrew, Swanson, and Williams, *Proc. Phys. Soc.* **77**, 36 (1961).
- ⁷⁶ E. R. Andrew and D. P. Tunstall, *Proc. Phys. Soc.* **78**, 1 (1961).
- ⁷⁷ W. G. Proctor and W. A. Robinson, *Phys. Rev.* **102**, 1183 (1956).
- ⁷⁸ W. G. Proctor and W. A. Robinson, *Phys. Rev.* **104**, 1344 (1956).
- ⁷⁹ W. G. Proctor and W. H. Tanttala, *Phys. Rev.* **98**, 1854 (1955).
- ⁸⁰ S. A. Al'tshuler, *DAN SSSR* **85**, 1235 (1952).
- ⁸¹ S. A. Al'tshuler, *JETP* **28**, 49 (1955), *Soviet Phys. JETP* **1**, 37 (1955).
- ⁸² S. A. Al'tshuler, *JETP* **28**, 38 (1955), *Soviet Phys. JETP* **1**, 29 (1955).
- ⁸³ Bloembergen, Shapiro, Pershan, and Artman, *Phys. Rev.* **114**, 445 (1959).
- ⁸⁴ L. B. Robinson, *Canad. J. Phys.* **35**, 1344 (1957).
- ⁸⁵ Hockenberry, Brown, and Williams, *J. Chem. Phys.* **28**, 367 (1958).
- ⁸⁶ Hatton, Rollin, and Scymour, *Phys. Rev.* **83**, 672 (1951).
- ⁸⁷ W. G. Segleken and H. C. Torry, *Phys. Rev.* **98**, 1537 (1955).
- ^{87a} R. Burnes, *J. Chem. Phys.* **32**, 1586 (1960).
- ⁸⁸ Casabella, Bray, and Barnes, *J. Chem. Phys.* **30**, 1393 (1959).
- ⁸⁹ T. P. Das, *J. Chem. Phys.* **27**, 1 (1957).
- ⁹⁰ G. Wessel, *Phys. Rev.* **92**, 1581 (1953).
- ⁹¹ Gordy, Ring, and Bury, *Phys. Rev.* **78**, 512 (1950).
- ⁹² H. Denmelt, *Z. Phys.* **134**, 642 (1953).
- ⁹³ H. Denmelt, *Z. Phys.* **133**, 528 (1952).
- ⁹⁴ K. S. Pennington and H. E. Petch, *J. Chem. Phys.* **33**, 329 (1960).

- ⁹⁵ F. Halui and H. E. Petch, *Canad. J. Phys.* **38**, 515 (1960).
- ⁹⁶ A. H. Silver and P. J. Bray, *J. Chem. Phys.* **29**, 984 (1958).
- ⁹⁷ A. H. Silver and P. J. Bray, *J. Chem. Phys.* **31**, 247 (1959).
- ⁹⁸ A. H. Silver and P. J. Bray, *J. Chem. Phys.* **32**, 288 (1960).
- ⁹⁹ A. H. Silver, *J. Chem. Phys.* **32**, 959 (1960).
- ¹⁰⁰ N. Knight, *Phys. Rev.* **92**, 539 (1953).
- ¹⁰¹ N. A. Schuster and G. E. Pake, *Phys. Rev.* **81**, 886 (1951).
- ¹⁰² R. F. Kiddle and W. G. Proctor, *Phys. Rev.* **104**, 932 (1956).
- ¹⁰³ H. G. Cox and D. Williams, *J. Chem. Phys.* **32**, 633 (1960).
- ¹⁰⁴ G. Becker, *Z. Phys.* **130**, 171 (1951).
- ¹⁰⁵ H. Krüger and Y. Meyer-Berkhout, *Z. Phys.* **132**, 171 (1952).
- ¹⁰⁶ R. White, *J. Chem. Phys.* **23**, 253 (1954).
- ¹⁰⁷ G. Harrmann, *J. Chem. Phys.* **29**, 875 (1958).
- ¹⁰⁸ Katudat and Pound, *J. Chem. Phys.* **26**, 708 (1957).
- ¹⁰⁹ J. Biorkstam and E. A. Uehling, *Phys. Rev.* **114**, 961 (1959).
- ¹¹⁰ R. Berson, *J. Chem. Phys.* **32**, 85 (1960).
- ¹¹¹ P. Kaplan and E. L. Hahn, *Bull. Am. Phys. Soc.* **2**, 384 (1957).
- ¹¹² J. E. Hon and P. J. Bray, *Phys. Rev.* **110**, 624 (1958).
- ¹¹³ Murakami and Hirakara, *J. Phys. Soc. Japan* **11**, 607 (1956).
- ¹¹⁴ E. Harris and M. Melkanoff, *Phys. Rev.* **90**, 585 (1953).
- ¹¹⁵ S. L. Kahalas and R. K. Nesbet, *Phys. Rev. Letts.* **6**, 549 (1961).
- ¹¹⁶ N. G. Cranna, *Canad. J. Phys.* **31**, 1185 (1953).
- ¹¹⁷ C. T. O'Konski and T. J. Flouitt, *J. Chem. Phys.* **27**, 815 (1957).
- ¹¹⁸ M. Minematsu, *J. Phys. Soc. Japan* **14**, 1030 (1959).
- ¹¹⁹ P. A. Casabella and P. J. Bray, *J. Chem. Phys.* **28**, 1182 (1958).
- ¹²⁰ P. A. Casabella and P. J. Bray, *J. Chem. Phys.* **29**, 1105 (1958).
- ¹²¹ Casabella, Bray, and Negita, *J. Chem. Phys.* **32**, 314 (1960).
- ¹²² H. Negita and P. J. Bray, *J. Chem. Phys.* **33**, 1876 (1960).
- ¹²³ S. Kojima and M. Minematsu, *J. Phys. Soc. Japan* **15**, 355 (1960).
- ¹²⁴ J. Itoh and R. Kusaka, *J. Phys. Soc. Japan* **9**, 209 (1954).
- ¹²⁵ F. Haluj and H. E. Petch, *Canad. J. Phys.* **34**, 1169 (1956).
- ¹²⁶ A. Weiss, *Z. Naturforsch.* **152**, 536 (1960).
- ¹²⁷ Brun, Hofner, and Hartmann, *Helv. Phys. Acta* **33**, 495 (1960).
- ¹²⁸ Brun, Hofner, and Hartmann, *Helv. Phys. Acta* **33**, 496 (1960).
- ¹²⁹ R. M. Cotts and W. D. Knight, *Phys. Rev.* **96**, 1285 (1954).
- ¹³⁰ Eades, Hugers, and Andrew, *Proc. Phys. Soc.* **71**, 1019 (1958).
- ¹³¹ R. R. Hewitt, *Phys. Rev.* **121**, 45 (1961).

Translated by J. G. Adashko